The 2021 outburst of the recurrent nova RS Ophiuchi observed in X-rays by the *Neil Gehrels Swift Observatory*: a comparative study

K. L. Page [1]*, A. P. Beardmore [1], J. P. Osborne,[1] U. Munari [2], J.-U. Ness,[3] P. A. Evans [1], M. F. Bode,[4,5] M. J. Darnley [4], J. J. Drake,[6] N. P. M. Kuin,[7] T. J. O'Brien,[8] M. Orio [9,10] S. N. Shore,[11,12] S. Starrfield[13] and C. E. Woodward[14]

[1]*School of Physics and Astronomy, University of Leicester, Leicester LE1 7RH, UK*
[2]*INAF – National Institute of Astrophysics, I-36012 Asiago, Italy*
[3]*European Space Agency (ESA), European Space Astronomy Centre (ESAC), Camino Bajo del Castillo s/n, E-28692 Villanueva de la Cañada, Madrid, Spain*
[4]*Astrophysics Research Institute, Liverpool John Moores University, IC2 Liverpool Science Park, Liverpool L3 5RF, UK*
[5]*Vice Chancellor's Office, Botswana International University of Science and Technology, Private Bag 16, Palapye, Botswana*
[6]*Harvard-Smithsonian Center for Astrophysics, 60 Garden Street, Cambridge, MA 02138, USA*
[7]*Mullard Space Science Laboratory, University College London, Holmbury St Mary, Dorking, Surrey RH5 6NT, UK*
[8]*Jodrell Bank Centre for Astrophysics, University of Manchester, Alan Turing Building, Manchester M13 9PL, UK*
[9]*Department of Astronomy, University of Wisconsin-Madison, 475 N Charter Street, Madison, WI 53706, USA*
[10]*INAF – Padova, Vicolo dell'Osservatorio 5, I-35122 Padova, Italy*
[11]*Dipartimento di Fisica 'Enrico Fermi', Università di Pisa, I-56127 Pisa, Italy*
[12]*INFN – Sezione Pisa, Largo Bruno Pontecorvo 3, I-56127 Pisa, Italy*
[13]*Earth and Space Exploration, Arizona State University, PO Box 871404, Tempe, AZ 85287-1404, USA*
[14]*Minnesota Institute for Astrophysics, University of Minnesota, 116 Church Street SE, Minneapolis, MN 55455, USA*

ABSTRACT

On 2021 August 8, the recurrent nova RS Ophiuchi (RS Oph) erupted again, after an interval of 15.5 yr. Regular monitoring by the *Neil Gehrels Swift Observatory* began promptly, on August 9.9 (0.37 d after the optical peak), and continued until the source passed behind the Sun at the start of November, 86 d later. Observations then restarted on day 197, once RS Oph emerged from the Sun constraint. This makes RS Oph the first Galactic recurrent nova to have been monitored by *Swift* throughout two eruptions. Here we investigate the extensive X-ray data sets between 2006 and 2021, as well as the more limited data collected by the *European X-ray Observatory Satellite* (*EXOSAT*) in 1985. The hard X-rays arising from shock interactions between the nova ejecta and red giant wind are similar following the last two eruptions. In contrast, the early supersoft source (SSS) in 2021 was both less variable and significantly fainter than in 2006. However, 0.3–1 keV light curves from 2021 reveal a 35 s quasi-periodic oscillation consistent in frequency with the 2006 data. The *Swift* X-ray spectra from 2021 are featureless, with the soft emission typically being well parametrized by a simple blackbody, while the 2006 spectra showed much stronger evidence for superimposed ionized absorption edges. Considering the data after day 60 following each eruption, during the supersoft phase the 2021 spectra are hotter, with smaller effective radii and lower wind absorption, leading to an apparently reduced bolometric luminosity. We explore possible explanations for the gross differences in observed SSS behaviour between the 2006 and 2021 outbursts.

Key words: stars: individual: RS Oph – novae, cataclysmic variables – X-rays: stars.

1 INTRODUCTION

Novae are the most energetic category of accreting white dwarfs (WDs). They occur in interacting binary systems, within which mass transfer from the donor (secondary) star forms a layer of hydrogen on the WD (primary) surface. When enough material has been accreted, nuclear burning ignites at the base of the envelope, and, once sufficient pressure has built up, a thermonuclear runaway (TNR) begins (see review articles in Bode & Evans 2008; Woudt & Ribeiro 2014). The nova explosion expels material that initially obscures the

WD surface from view. However, as the ejecta expand, they become optically thin, thus allowing any continuing nuclear burning on the WD to become visible. This emission ultimately peaks in the soft X-ray band, and is known as the supersoft source (SSS) state (e.g. Krautter 2008). The launch of the *Neil Gehrels Swift Observatory* (*Swift* hereafter; Gehrels et al. 2004) has led to this SSS phase being well monitored in many novae (see Osborne 2015; Page, Beardmore & Osborne 2020, for recent reviews), revealing previously unseen phenomena, such as high-amplitude flux variability and short time-scale quasi-periodic modulations.

Classical novae (CNe) are those that have only been seen to erupt once. A small number of systems, however, have been detected in

outburst multiple times, and these are known as recurrent novae (RNe). There are 10 confirmed Galactic recurrents, of which the subject of this paper, RS Ophiuchi (RS Oph hereafter), is one. It is believed that all novae should eventually recur, but most over periods of thousands of years (Yaron et al. 2005 discuss the parameter space of nova outbursts). The Galactic RNe have recurrence time-scales of ∼10–100 yr (the upper bound being a selection effect dependent on historical records), while some RNe outside our own Galaxy have been found to recur as frequently as every year (e.g. Darnley et al. 2014). Reviews of the recurrent novae in the Milky Way are provided by Schaefer (2010) and Darnley (2021).

The RS Oph system comprises a massive WD and a red giant (RG) donor. The mass range estimate for the WD is 1.2–1.4 $M_\odot$ (e.g. Mikołajewska & Shara 2017), and the orbital period, P_{orb}, of the binary is 453.6 ± 0.4 d (Brandi et al. 2009). Using the ephemeris in that paper, the eruption times in 2006 and 2021 are separated by (12.47 ± 0.01)P_{orb} – that is, the orbital phase is close to 180° different between the two outbursts; the 1985 eruption occurred at approximately the same phase as in 2006. The RS Oph WD and RG were in quadrature at each of these times (phases 0.26 and 0.72, respectively, where phase 0.0 is defined to be inferior conjunction of the RG).

RS Oph has previously passed through nova eruption cycles approximately every 15 yr, with a range spanning 9–27 yr (see Schaefer 2010, for a summary), having been first detected as a nova in 1898 (Pickering 1905). This short recurrence time suggests the system contains a massive WD, accreting at a substantial rate. Prior to 2021, the previous eruption occurred in 2006 February, and this was the first nova monitored in detail by *Swift*, leading to an exquisite data set that was published by Bode et al. (2006) and Osborne et al. (2011). The detailed *Swift* results in 2006 revealed absorbed, hard X-rays early after the eruption, with the absorbing column decreasing and the temperature declining over the first few weeks. These spectra were explained as thermal emission from hot, shocked gas, as the nova ejecta interacted with the RG wind (Bode et al. 2006). On day 26, a new, very soft component was detected, signifying the beginning of the SSS phase. This soft emission was extremely variable in flux for almost 3 weeks, before settling at a consistently bright level until around day 60, when a monotonic decline set in.

Collimated bipolar structures (jets) were detected following the 2006 eruption (e.g. O'Brien et al. 2006; Bode et al. 2007; Sokoloski, Rupen & Mioduszewski 2008; Montez et al. 2022), highlighting the lack of spherical symmetry during the explosion (see also models by Walder, Folini & Shore 2008; Orlando, Drake & Laming 2009). No eclipses are seen in RS Oph, placing limits on the angle of inclination, with estimates ranging from 30° to 52° (Dobrzycka & Kenyon 1994; Brandi et al. 2009; Ribeiro 2012).

RS Oph was reported to have erupted again on 2021 August 8, as described in the American Association of Variable Star Observers (AAVSO) Alert Notice 752.[1] This prompted a flurry of observations across the electromagnetic spectrum, from very high energy TeV/GeV γ-rays detected by the High Energy Stereoscopic System (H.E.S.S.; Wagner 2021a,b; H. E. S. S. Collaboration et al. 2022) and Major Atmospheric Gamma Imaging Cherenkov Telescopes (MAGIC; Acciari et al. 2022), and MeV γ-rays by *Fermi*-Large Area Telescope (LAT; Cheung, Ciprini & Johnson 2021a; Cheung et al. 2021b, 2022); to X-rays seen by *Monitor of All-sky X-ray Image* (*MAXI*; Shidatsu et al. 2021), *INTErnational Gamma-*

Ray Astrophysics Laboratory (*INTEGRAL*; Ferrigno et al. 2021), *Neutron Star Interior Composition Explorer* (*NICER*; Enoto et al. 2021a,b; Luna et al. 2021; Orio et al. 2021b,c), *Nuclear Spectroscopic Telescope Array* (*NuSTAR*; Luna et al. 2021), *AstroSat* (Rout et al. 2021), *Chandra*, and *XMM–Newton* (Orio et al. 2021a), as well as *Swift* (Page 2021a,b; Page, Osborne & Aydi 2021); to optical (Fajrin et al. 2021; Mikolajewska et al. 2021; Munari & Valisa 2021a,b; Munari, Valisa & Ochner 2021; Nikolov & Luna 2021; Ricra, Vannini & Baella 2021; Shore et al. 2021a,c; Shore, Teyssier & Thizy 2021b; Taguchi, Ueta & Isogai 2021a; Taguchi et al. 2021b; Zamanov et al. 2021); infrared (Woodward et al. 2021a,b); and radio (Peters et al. 2021; Sokolovsky et al. 2021; Williams et al. 2021). A neutrino search was performed by IceCube, though only upper limits could be placed (Pizzuto, Vandenbroucke & Santander 2021).

In this paper, we present the *Swift* X-ray observations of the 2021 outburst of RS Oph, and compare them to the data obtained following the 2006 eruption, finding significant differences over the soft X-ray band, while the harder X-rays are much more similar. We focus mainly on the SSS emission, while Cheung et al. (2022) present a discussion of the higher energy shock emission alongside the LAT results.

Despite the well-known close similarity between the optical light curves of individual RNe (e.g. Schaefer 2010), the SSS phase can sometimes show wider variations from one outburst to the next. For example, the yearly recurrent M31N 2008-12a showed very similar (optically identical) multiwavelength results from 2008 to 2021, with the exception of the 2016 eruption, which was notably different in X-rays (Henze et al. 2018; Healy et al., in preparation). Nova LMC 1968 has also been observed by *Swift* through two eruptions (2016 and 2020), in both cases showing very similar X-ray (and optical) evolution (Kuin et al. 2020; Schwarz et al. 2020). RS Oph is the first Galactic recurrent for which this comparison has been possible;[2] it is also one of the brightest RNe in the X-ray band, thus allowing a detailed examination.

Throughout this paper, errors are given at the 1σ confidence level, unless otherwise stated. Spectra were binned such that they have a minimum of 1 count bin^{-1} to facilitate Cash statistic (Cash 1979) fitting within XSPEC (Arnaud 1996), and the abundances from Wilms, Allen & McCray (2000), together with the photoelectric absorption cross-sections from Verner et al. (1996), have been assumed when using the Tübingen–Boulder interstellar medium (ISM; XSPEC/TBABS) absorption model.

For ease of comparison with the previous publications for the *Swift* 2006 data, the time origin of the light curves presented here, $T0$, has been taken as the time at which the optical emission peaked; this is estimated to be 2021 August 09.542 UT (MJD 59435.542) from the AAVSO light curve.[3] For 2006, $T0$ (again, the time of optical maximum) is taken to be 2006 February 12.83 UT (Hirosawa 2006). We also assume a distance of 1.6 kpc (Bode 1987). The parallax determined by *Gaia* corresponds to a greater distance of $2.4^{+0.3}_{-0.2}$ kpc (Bailer-Jones et al. 2021), but Schaefer (2018) notes that

---

[2] We note that it appears that the latest eruption of U Sco might have occurred during solar conjunction in 2017, and was thus entirely missed (Schaefer, private communication), otherwise this event would also have been observed by *Swift*.

[3] For the LAT data analysis, Cheung et al. (2022) have assigned $T0$ to be the start time of the eruption from Munari & Valisa (2021c), 1.04 d before our optical peak time.
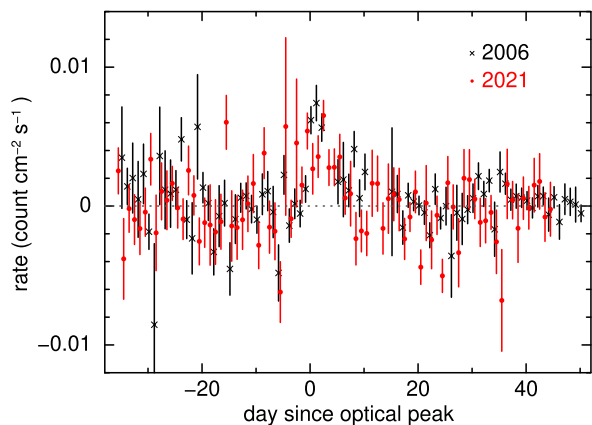
Figure 1. BAT data from the transient monitor, showing a faint, but clear, detection of RS Oph over 15–50 keV in both 2006 (black crosses) and 2021 (red circles). The abscissa shows days since the peak in the optical light curve for each eruption. The horizontal dotted line marks the zero count rate level.

these parallaxes are not yet reliable for systems with long-period binary orbits, and can lead to either under- or overestimates of the distance. See Montez et al. (2022) and Acciari et al. (2022) for recent discussions on the distance to RS Oph.

2 OBSERVATIONS

Following a target of opportunity request promptly after the announcement of the new eruption, *Swift* observations began on 2021 August 9.9, only 0.37 d after the optical peak (1.41 d after the probable start time of the nova event; Munari & Valisa 2021c). Initially, observations were performed on a daily basis; from the start of September, the cadence was increased to every 12 h, then to every 8 h between September 15 and October 1. Daily observations then resumed until RS Oph entered the *Swift* solar observing constraint on November 5. In addition, on September 12 observations were taken every *Swift* orbit (approximately every 1.5 h); this date was chosen as a time corresponding to the number of days (∼33) after the 2006 eruption when high-amplitude soft-flux variability was seen. These observations were all obtained using the X-Ray Telescope (XRT; Burrows et al. 2005) Windowed Timing (WT) mode, since the count rate was consistently above 1 count s^{-1}. There were, in addition, a number of separate observations performed in Photon Counting (PC) mode between September 24 and October 8; these were taken to investigate possible extended emission around the source. Given the extreme level of pile-up in these PC observations, the data are not considered in this paper.

Photometric and grism data were also collected using the *Swift* Ultraviolet/Optical Telescope (UVOT; Roming et al. 2005). These results will be presented in a separate publication. In addition, the Burst Alert Telescope (BAT; Barthelmy et al. 2005) transient monitor[4] (Krimm et al. 2013) showed an apparent weak detection of RS Oph over 15–50 keV for a few days (Fig. 1) around the time of the eruption (as was the case in 2006; Bode et al. 2006).

Fig. 2 shows the optical data collected by the Asiago Novae and Symbiotic Stars (ANS) Collaboration during both 2021 and 2006 (see Munari et al. 2007, for a summary of the 2006 results). The light curves and colour evolution from the two eruptions appear almost identical. It can be seen that, at the time RS Oph entered solar
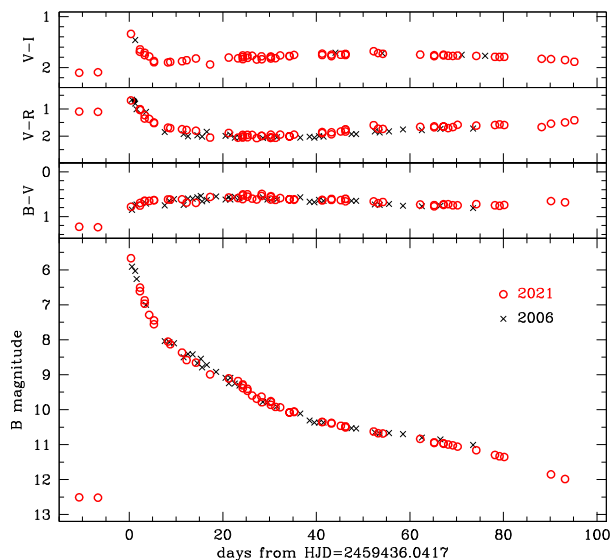
Figure 2. *B*-band photometry and colour diagrams from the ANS Collaboration, from both 2021 and 2006. The two outbursts are almost identical at optical wavelengths.

conjunction in 2021, on day 86, the system had not yet returned to the pre-eruption brightness, still being around half a magnitude brighter in *B*.

The flux of the optical [Fe X] 6375 Å coronal line was measured from the RS Oph spectral atlas by Munari & Valisa (2021c, 2022), which provides absolute fluxed spectra (primarily Echelle) obtained at nearly daily cadence. These results are discussed in Section 4.1.2.

The *Swift*-XRT data were analysed with HEASOFT 6.29 and the most up-to-date calibration files available at the time (release date of 2021 September 23). Only grade 0 (single pixel) events were utilized, in order to help minimize optical loading.[5] We note that the 2006 data presented in Osborne et al. (2011) used WT grades 0–2 (at that time our understanding of the best way to mitigate optical loading was less complete than it is today). The 2006 light curves and spectra presented here have also been reprocessed with the latest software and only grades 0 considered; the results are not materially different from Osborne et al. (2011), however.

3 X-RAY LIGHT CURVE

Light curves for both the 2006 and 2021 data sets were generated using the online XRT product generator[6] (Evans et al. 2007, 2009). Looking at the shape of the spectra, 1 keV was chosen as a suitable cut between the SSS component and the harder, shock-related emission. Fig. 3 shows the light curves over the soft (0.3–1 keV) and hard (1–10 keV) bands, together with the hardness ratios (defined as the ratio of the counts in the 1–10 keV and 0.3–1 keV bands) for the two eruptions. There are clearly some similarities between the data sets, particularly at earlier times before the start of the SSS phase, but, overall, the evolution of the soft-band light curve is markedly different, with the bulk of the 2021 SSS emission rising later, peaking at a lower level and then starting to fade earlier, before rebrightening briefly, compared with 2006.

---

[4]https://swift.gsfc.nasa.gov/results/transients/RSOph/

[5]https://www.swift.ac.uk/analysis/xrt/optical_loading.php
[6]https://www.swift.ac.uk/user_objects/
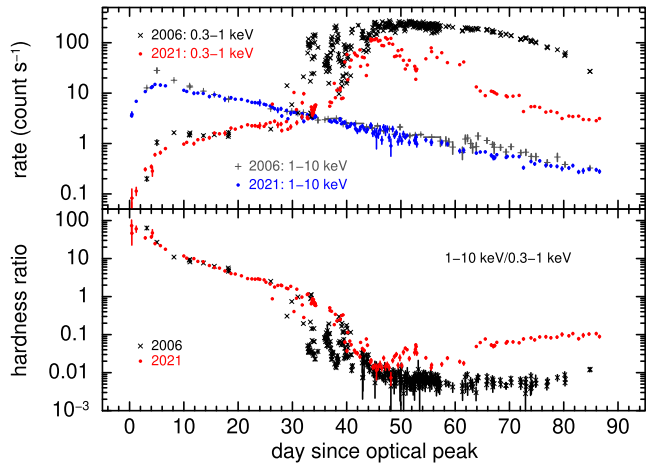
Figure 3. Top: a comparison of the soft (0.3–1 keV: 2006 – black crosses; 2021 – red circles) and hard (1–10 keV: 2006 – grey pluses, 2021 – blue circles) light curves following the 2006 and 2021 eruptions. Bottom: the hardness ratios following the 2006 (black crosses) and 2021 (red circles) eruptions.
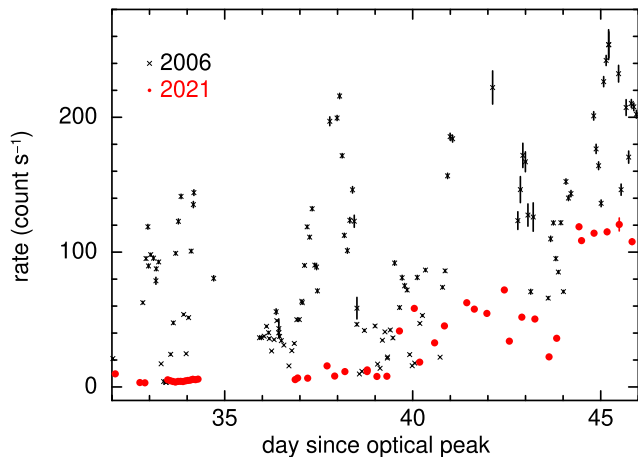
Figure 4. A comparison of the 2006 and 2021 0.3–1 keV light curves during the early supersoft phase. The 2006 data set reaches a higher count rate, and shows larger amplitude changes, though both data sets are variable. The peaks and troughs of the variability occur at different times in 2006 and 2021.

3.1 0.3–1 keV

Basing our expectations of the light-curve evolution on the results from 2006, and in order to put stringent limits on the start of the SSS in 2021, observations with at least a daily cadence were obtained from the very beginning of our monitoring campaign. The first hint of spectral softening appeared on day 20.6 (Page 2021a), with no sign of enhanced low-energy emission during the previous observation on day 19.5. This 'bump' in the spectrum stayed small until day 26.3, when the soft component increased significantly (Page 2021b). In 2006, (weak) soft emission was first detected on day 26.0, with an obvious increase in counts below 1 keV on day 29.0 (Osborne et al. 2011). Before this, the previous observation occurred 8 d earlier, on day 18.2. Therefore, although the 2021 SSS was noted a few days earlier than in 2006, this may simply be due to the denser sampling of the more recent eruption.

The onset of the SSS in 2006 was, however, much more dramatic than in 2021. Fig. 4 zooms in on the soft light curve between days

32 and 46, during which time the 2006 data showed high-amplitude flux variability, with changes in X-ray count rate of more than an order of magnitude in ∼12 h (see also Osborne et al. 2011). While the 2021 observations did show variability, Fig. 4 shows this was at a significantly lower level, with a peak count rate less than half that measured in 2006. It is clear that the timing of peaks and troughs in 2006 and 2021 is not the same. This is expected if the flux variability is caused by absorption in random, clumpy ejecta, which was discussed as a possibility by Osborne et al. (2011).

The other big difference, as shown in Fig. 3, is that the 2021 soft X-ray emission showed a definite fading trend between days ∼48 and 53, decreasing from around 100 to ∼20 counts s^{-1}, before rebrightening again over a few days. In 2006, the X-rays stayed consistently bright between days 46 and 58, after which time a steady decline set in (Osborne et al. 2011). As RS Oph entered the solar observing constraint in 2021 (day 87), the 0.3–10 keV XRT count rate was ∼3.4 counts s^{-1}, while the count rate on the corresponding day in 2006 was ∼20 counts s^{-1}.

The apparent rate of decline of the 2021 soft X-rays was also noticeably slower than the 2006 data at this late time: approximating the decay between days 75 and 85 with a power law[7] of $t^{-\alpha}$, the 2021 data can be fitted with $\alpha \sim 4.5$, while the 2006 light curve follows $\alpha \sim 11.5$. If instead we consider all the data after day 62 (after which point both light curves show a monotonic fading), the 2021 data decay can be approximated with a single power law of $\alpha \sim 5.1$ (although the data show considerable scatter), while the 2006 light curve shows a break in its fading, with $\alpha \sim 3.6$ until day 76, then steepening to ∼11.5.

By comparison of the light curves, we estimate the integrated number of observed soft (0.3–1 keV) X-ray counts between days 30 and 86 in 2006 was about 4–5 times larger than in 2021.

3.1.1 QPO

The 2006 eruption of RS Oph revealed a strong ∼35 s quasi-periodic oscillation (QPO) during the SSS phase (Beardmore et al. 2008; Osborne et al. 2011). Short-period oscillations were subsequently also identified in other bright novae observed by *Swift*, with time-scales of up to ∼100 s (e.g. KT Eri – Beardmore et al. 2010; V339 Del – Beardmore, Osborne & Page 2013; and V5668 Sgr – Page, Beardmore & Osborne 2015), and were confirmed in *XMM–Newton* and *Chandra* observations (Ness et al. 2015).

In order to search for similar oscillations from the current outburst, we extracted light curves from the WT data at 0.1 s binning in the 0.3–1 keV energy band, and applied a standard fast Fourier transform algorithm to calculate periodograms from individual snapshots (i.e. continuous on-target pointings) and their average (e.g. Leahy et al. 1983; van der Klis 1988; Vaughan et al. 2003). The periodograms were normalized following Leahy et al. (1983), so have predictable Poisson noise properties allowing the significance of potential signals to be evaluated. A maximum likelihood periodogram fitting technique was then applied (e.g. Barret & Vaughan 2012) to identify the QPO parameters. Given the mean duration of the light curves from each snapshot was ∼700 s, and ranged from 380 to 1250 s, the periodograms were computed over 700 s continuous time bins and padded to this duration with the mean snapshot count rate if they were shorter.

---

[7]Using a power law is simply a numerical convenience, without any physical implication.
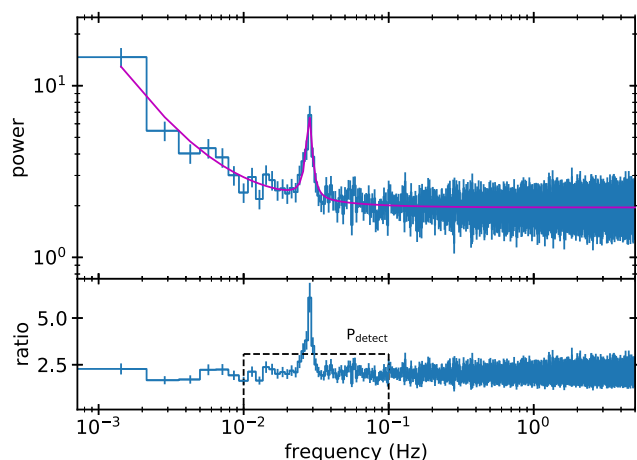
Figure 5. The upper panel shows the average of 59 periodograms (each spanning 700 s) from the 2021 WT data over days 36.87–61.56 (the main SSS interval), fitted with the model described in the text (magenta line). The bottom panel shows the ratio obtained between the average and model when the Lorentz (QPO) term is removed. The dashed line shows the 99 per cent detection level over the frequency range 0.01–0.10 Hz (i.e. periods of 10–100 s).

The average periodogram from days 36.87 to 61.56 covering the SSS bright phase is shown in Fig. 5. The 35 s modulation is clearly detected once more at greater than 99 per cent confidence. By fitting the periodogram with a model consisting of a power law (for the low frequency variations), a constant (for Poisson noise) and a Lorentzian (for the QPO), a best-fitting oscillation frequency of 28.31 ± 0.21 mHz was obtained, corresponding to a period of 35.33 ± 0.26 s, with a fractional rms of 1.94 ± 0.2 per cent. The best-fitting width of the Lorentzian corresponds to an average coherence of 7.7 ± 1.8 cycles. The QPO was not detected before or after days 36.87–61.56. Examination of the individual periodograms shows the QPO was detected in approximately 20 per cent of this interval. The maximum amplitude seen in any individual periodogram was 5 per cent. *NICER* also reported the detection of a $\sim$35 s oscillation (Orio et al. 2021b).

During the 2006 outburst, the XRT measured an average best-fitting period of 35.04 ± 0.09 s, a fractional rms of 2.43 ± 0.20, and coherence of 20.9 ± 2.4 cycles (Beardmore et al., in preparation will provide a full analysis of the 2006 data). Thus, while the QPO was not so strongly detected in 2021 (probably due in part to the shorter snapshots of data obtained, as well as the source being fainter), the periods are entirely consistent.

3.2 1–10 keV

In comparison with the large differences over the 0.3–1 keV band between the two eruptions, the 1–10 keV X-rays were much more consistent, in terms of both brightness and evolution, as Fig. 3 shows. The 2021 *Swift* observations began almost 3 d earlier than in 2006, giving us a firmer handle on the initial rise of the X-rays. The harder emission was seen to increase in strength until around day 5 following both eruptions, though the 2021 peak 1–10 keV count rate is only about half that seen in 2006. (The higher cadence of observations in 2021 makes the peak time better defined.) The 2006 data then faded more rapidly until around day 15–20 (following an approximate power-law decay of $\alpha \sim 1$, compared with 0.5 for the 2021 data), at which point both the count rate

and rate of decline became very similar to what we see in 2021 ($\alpha \sim 2$). There is an interval between days 60 and 70 where the 2006 data showed a slight excess compared with 2021 but, overall, the 1–10 keV light curves are rather similar between the two nova events, especially in comparison with the differences in the soft emission.
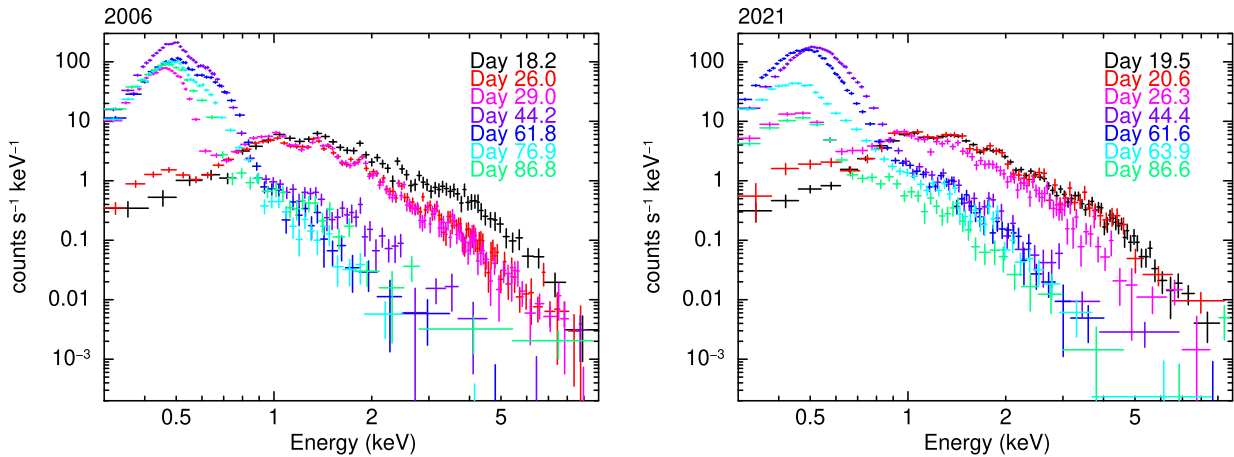
4 X-RAY SPECTRUM

Fig. 6 shows samples of X-ray spectra obtained during the 2006 and 2021 eruptions. The 2021 spectra show a very smooth, featureless supersoft component, which can be simply modelled by a blackbody (BB) component – occasionally improved by the inclusion of absorption edge(s), though often well modelled without. While Osborne et al. (2011) parametrized the 2006 data by use of an atmosphere component (the Tübingen non-local-thermodynamic-equilibrium model atmospheres; Rauch 2003), a BB+edges model also provides an acceptable fit to these 2006 data – in most cases, statistically better. In addition, the model atmospheres seemed unstable within XSPEC, with the fitted temperatures appearing almost quantized at certain values, despite small step sizes for fitting, and the minimization routine implemented. Given that high-resolution observations of novae have shown that the currently available atmosphere models do not account for all the complexities seen (Ness 2020), we have chosen to use the BB option for a direct comparison between the two eruptions. Fig. 7 demonstrates the better fit results obtained using a pure BB compared to the Tübingen grid 003 model atmosphere (as used in Osborne et al. 2011), particularly between 0.7 and 1 keV. The best fits for these two models applied to this example spectrum are $kT_{BB} = 43 \pm 1$ eV, $R_{BB} = (3.9^{+0.6}_{-1.8}) \times 10^{10}$ cm, $N_{H, BB} = (2.6^{+0.2}_{-0.3}) \times 10^{21}$ cm^{-2}, and $kT_{atmos} = 70 \pm 1$ eV, $R_{atmos} = (1.0 \pm 0.3) \times 10^{10}$ cm, $N_{H, atmos} = (2.9 \pm 0.2) \times 10^{21}$ cm^{-2}, respectively.

Looking in detail at the appropriate temperature Rauch atmosphere models, we determined that the strongest edges were those associated with He- and H-like N at 0.552 and 0.667 keV, and He- and H-like O at 0.739 and 0.871 keV. However, the energy dependence of the edge profiles in these grid models is very different from those implemented by the standard edge model in XSPEC, which assumes an E^{-3} cross-section above the edge. From the atmosphere models, we find a flatter dependence of E^{+1} is more appropriate at the temperatures of interest for RS Oph, so a local XSPEC model was defined to implement this different edge shape.[8] The differences are shown in Fig. 8. Additionally, the atmosphere models have absorption lines that may overlap/interact with the edges, one of which (H-like O at 0.654 keV) shifts the 0.667 keV edge energy to 0.635 keV at XRT CCD level spectral resolution.

All four of these edges were implemented in our model (using the E^{+1} shape). The optical depths of the edges accounting for He- and H-like N (0.552 and 0.635 keV) and He-like O (0.739 keV) were allowed to vary over a range of $\tau = 0$–5. The optical depth of the fourth edge (H-like O at 0.871 keV) included in the fit was fixed at 2; while this edge often improved the residuals, the overlap of the BB and cooler optically thin component (see below) made constraining the depth difficult.

The high-resolution grating spectra obtained following the 2006 eruption show both absorption and emission lines superimposed on

---

[8]Our cross-section energy dependence changes both the edge depth and the post-edge spectrum compared to the standard E^{-3} profile; while trends within our fits can be informative, direct comparisons with model fits using standard edges will not be meaningful.
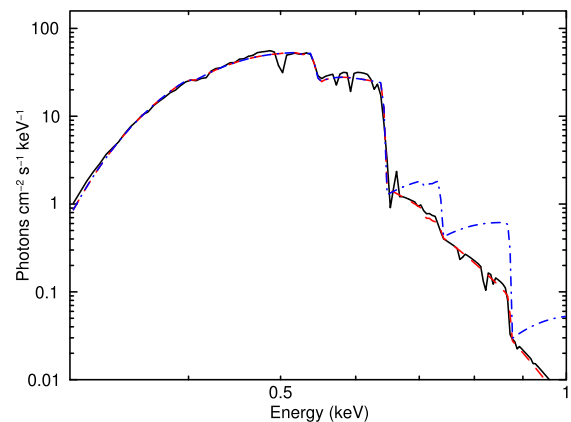
Figure 6. Evolution of the X-ray spectra through the 2006 (left) and 2021 (right) eruptions. Left: 2006 spectra. The black spectrum shows the last date when there was no detectable SSS emission, on day 18.2, while the red shows the first where a soft excess was seen, on day 26.0, 8 d later. The next observation occurred on day 29, and showed a strong soft component. Days 44.2, 61.8, and 86.8 are shown for direct comparison with the 2021 results on those days (see right-hand plot and description below). Since there was no sudden drop in observed count rate between days 61.6 and 63.9 in 2006, the spectrum from day 76.9 is included instead. Right: 2021 spectra. The black spectrum again shows the last date when there was no detectable SSS emission, on day 19.5; the next observation, in this case taken only 27 h later, showed a slight increase in counts below ∼0.6 keV. The slightly enhanced soft emission stayed around this level until day 26.3, when an obvious soft component appeared. The X-ray count rate reached a peak around day 44.4, after which there was a decline followed by a rebrightening. Because of the proximity of RS Oph to the Moon, the source could not be observed between days 61.6 and 63.9, during which time the count rate dropped from ∼41.5 to ∼14 counts s^{-1} (blue and cyan spectra). The blue/green spectrum corresponds to the last day RS Oph could be observed before entering the Sun constraint.
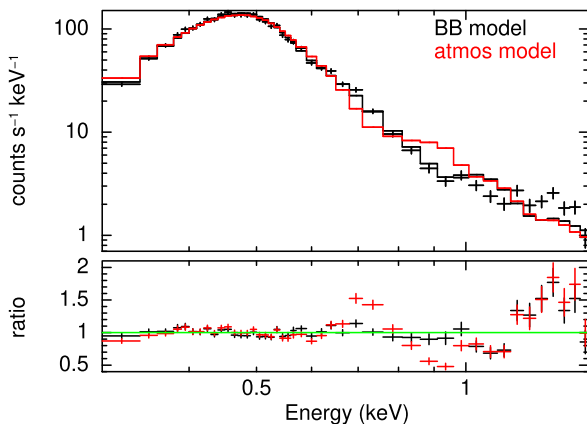
Figure 7. Comparison of the BB (with no absorption edges; $kT = 43 \pm 1$ eV) and atmosphere fits (using Rauch grid 003; $kT = 70 \pm 1$ eV) to the SSS emission on day 43.8 of the 2021 eruption. The bottom panel plots the ratio of the data to both models; this clearly shows the fit deficiency using the Rauch grid 003 atmosphere model in the interval 0.7–1 keV.


Figure 8. Comparison of the Rauch atmosphere grid (solid black line), the BB model including standard XSPEC edges following E^{-3} dependence (blue dot–dashed lines; this is not an actual fit to the data, but aligned to show the different edge shapes clearly), and the BB model including edges with an E^{+1} recovery (red dashed lines). In the model used for this example, only additional edges at 0.635, 0.739, and 0.871 keV were significant; the dip close to 0.55 keV is simply due to the interstellar absorption modelled by TBABS, so the shape does not vary between the models.

the continuum (Ness et al. 2007a, 2009), as do the 2021 spectra (Ness et al., in preparation). Such lines are not required when modelling the lower resolution XRT spectra, though unmodelled emission lines at low energies could affect the fitted absorbing column. A quick comparison between the 2021 *XMM–Newton*/Reflection Grating Spectrometer (RGS) spectra and contemporaneous XRT spectra gives no great cause for concern at these low energies, however. Indeed, the fit parameters from the *Swift* data closest in time to the *XMM–Newton* observation on day 37 of the 2021 eruption, applied directly to those RGS spectra show that they are a reasonable approximation to the underlying continuum, with emission lines superimposed. Similarly, a comparison between contemporaneous XRT and *NICER* spectra (Orio et al., in preparation) shows general agreement.

We note that the resolution of the XRT WT mode at 0.5 keV is currently 115 eV (full width at half-maximum – FWHM), compared with 82 eV in 2006.[9] Sharp spectral features will therefore not be resolved in the *Swift* data.

In both 2006 and 2021, the harder (>1 keV) emission, due to the shocked wind, has been parametrized in this paper by two optically thin (APEC in XSPEC) components, fixed at solar abundance. Consid-

---

[9]The FWHM of 63 eV given in Osborne et al. (2011) was measured using an older response function (response matrix file – RMF). Since that work was published, the calibration was updated with a slightly broader response.
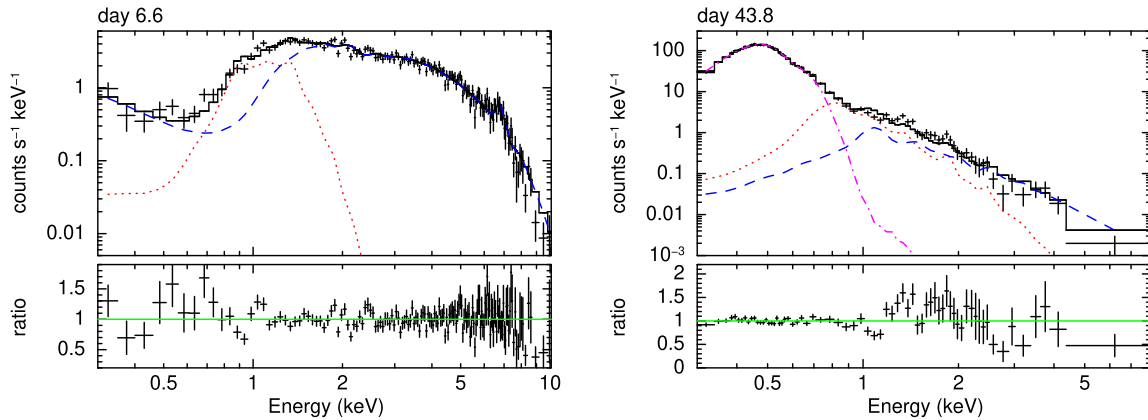
Figure 9. Example spectra demonstrating how well the models fit the 2021 data, before and during the SSS phase. Left-hand panel: spectrum from day 6.6 after the eruption, at the time the 1–10 keV emission peaked, fitted with two optically thin components (red and blue). Right-hand panel: spectrum from day 43.8 after the eruption, around the time the 0.3–1 keV emission peaked, fitted with a BB plus edges (magenta), together with two optically thin components (red and blue).

ering the pre-SSS shock data, there are no strong residuals suggesting non-solar abundances would improve the fits to the *Swift* spectra (see left-hand panel of Fig. 9). In some individual observations only one APEC was required at $\gtrsim$90 per cent confidence, while others could be improved by the inclusion of a third, cooler component (typically $\sim$100–200 eV). This is a simplification of what may physically be a more complex underlying shock continuum (see e.g. Vaytet, O'Brien & Bode 2007; Vaytet et al. 2011). However the two-temperature model accounts for the measured harder emission well.

Each spectrum was also attenuated by two absorption components: the ISM value fixed at 2.4×10^{21} cm^{-2} (Hjellming et al. 1986), and a variable column density due to the RG wind. In Osborne et al. (2011), this additional wind absorption was constrained to follow a power-law decline over time based on analysis in Bode et al. (2006). However, in the current analysis (both for the new 2021 observations, and the re-analysis of the 2006 data), we have chosen to allow this column to vary because of the apparently more complex variation seen with this larger sample of data. The oxygen abundance for the excess $N_{\rm H, wind}$ above the ISM level was fixed at 0.3 solar (within the XSPEC/TBFEO model). This lower oxygen abundance was determined from modelling the grating observations in 2006 (Ness et al. 2007a; Osborne et al. 2011), and typically provides an improvement when fitting the 2021 data sets as well, so was adopted throughout the analysis described below.

The same absorption parameter, $N_{\rm H, wind}$, was applied to all components in each fit; i.e. the soft, optically thick BB and harder optically thin components were absorbed by the same column. Although it is possible that the emission from the nuclear burning on the WD surface and that from shocks with the RG wind experience different levels of absorption, a single varying column (in excess of the fixed Galactic value) led to acceptable fits. This excess absorption has been assumed to be neutral.

Fig. 9 shows two example spectra from the times in 2021 where the 1–10 and 0.3–1 keV emission peaked, respectively, with the fitted components shown (red dots and blue dashes for the optically thin shock emission, and a magenta dot–dash line for the edge-absorbed BB component; in this example, only the He-like oxygen edge was significant). While the models are clearly not perfect, with some fit residuals apparent, the overall fit to the continuum is good (C-stat/degrees of freedom (dof) = 852/766 and 275/245, respectively, for the spectra plotted).

4.1 Spectral fitting results

Experimenting with different fits, it became clear that the ionized edges were much more significant in the 2006 spectra, with most of the 2021 soft data being well modelled with a BB alone. Indeed, upon fitting the 2021 spectra with different combinations of edges, it was apparent that there could be significant degeneracy between the edges included and the BB temperature for some of the spectra. That is, fits with a low ($\sim$50 eV) BB kT and shallow/no edges, or a higher kT ($\sim$100–150 eV) and deep edges, often lead to a very similar goodness of fit (C-stat values within $\sim$5 of each other), with little difference in the fit residuals.

The majority of the 2006 spectra were better fitted by including some or all of the four absorption edges described above. The left-hand panel of Fig. 10 demonstrates how the optical depths of the edges varied in the 2006 spectral fits; recall that the depth of the H-like O edge at 0.871 keV was fixed at $\tau = 2$ throughout. Of the three with variable optical depths, the He-like O edge at 0.739 keV was the most significant at early times. This optical depth then decreased, until about day 70, after which time the edge was no longer strongly significant. The 0.552 keV He-like N edge is the second deepest at the start of the SSS phase, also decreasing in strength with time, until becoming insignificant after around day 55. The edge at 0.635 keV, related to H-like N, was really only required after day 60, and its optical depth increased steadily after this time. No such obvious trends were found in the typically less significant optical depths in the 2021 fits, as can be seen in the right-hand panel of Fig. 10. Because of these findings, we choose to show both single BB fits, and those from a BB plus these four absorption edges (for the SSS emission) as described above; the underlying APEC components were included to account for the shock emission.

Figs 11 and 12 show the results of fitting the spectra with two absorbed optically thin APEC components before the onset of the SSS phase, then with a BB without and with absorption edges included as well, for both 2006 and 2021. In both cases, the top panel plots the observed 0.3–10 keV fluxes (in units of erg cm^{-2} s^{-1}) corresponding to the BB component (modelling the SSS; shown in black and red) and the combined APEC emission (modelling the underlying shocks; grey and blue). The second panel demonstrates the evolution of the temperatures of the two optically thin APEC components, while the third does the same for the BB, with the corresponding BB effective radius in the fourth. The bottom panel shows how the excess
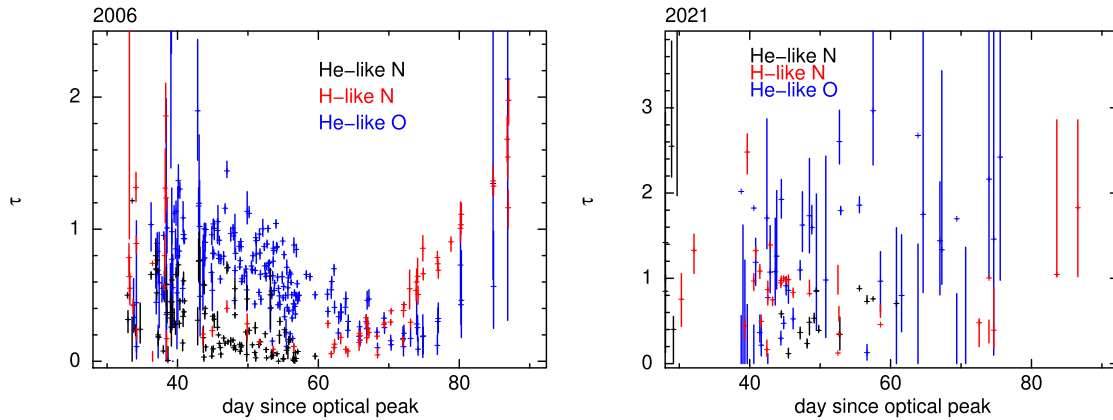
Figure 10. Plots of the fitted edge optical depths for which the 1σ lower limit is inconsistent with zero. For the 2006 data set (left), the He-like O edge (0.739 keV; blue) was the most significant at early times, decreasing in strength with time. The shallower optical depth of the He-like N (0.552 keV; black) edge followed a similar decreasing trend. H-like N (0.635 keV; red) improved the fits mainly after day 60. The optical depths of the edges fitted to the 2021 spectra (right) do not show any obvious trends. The small number of edges for which the optical depth pegged at the deepest allowed value of $\tau = 5$ have been omitted from the plots. Note that the vertical scales are different for the two plots.

absorbing column, $N_{\rm H, wind}$, decreases with time. In both plots, the axes in each corresponding panel are scaled to be the same, for ease of direct comparison. The fitted parameters corresponding to these figures are provided in Table 1.

At later times in 2021, there were intervals where the fitted BB temperature was seen to jump dramatically within a day; as discussed above, this is caused by the temperature/edge depth degeneracy. Given that most of the spectra were better fitted (albeit often only slightly) with the cooler ($\sim$50 eV) BBs, the sudden apparent jumps to higher temperatures are most probably anomalous, and not physical. For the fits to these spectra, the BB component was therefore fixed at the mean temperature of the two spectra before and after in time where the BB temperature was cooler; these data are plotted in magenta in Fig. 12, with the corresponding cooler/hotter APEC parameters shown in magenta/cyan. The optical depths of the edges shown in Fig. 10 correspond to these lower BB temperature fits.

4.1.1 Comparison between fits with and without absorption edges

The main differences seen when absorption edges are included in modelling the observed spectra are an increase in BB temperature (by 10–15 eV), and a decrease in the effective radius of the emitting region (by about a factor of 3), in both cases after day 40, once the SSS emission had settled down. To a lesser extent, there is also a slight decrease in the excess $N_{\rm H}$ over this same interval. All of these differences are clearer in the 2006 data, where the edges are more strongly detected.

4.1.2 Comparison between 2021 and 2006 fits

The underlying X-ray spectral shape was similar in both 2006 and 2021, with the temperatures and absorbing columns covering approximately the same parameter space, though with certain differences.

The temperatures of the two optically thin components, together with $N_{\rm H, wind}$, evolve most strongly during the first 10–15 d after the nova event, both in 2006 and 2021. Beyond this time, the shock emission cools slowly, and the measured absorbing column declines only a little further, although there is a drop in $N_{\rm H, wind}$ after day $\sim$ 60 in 2021. While a consistently higher absorbing column might

present itself as a simple explanation for the lower SSS flux observed in 2021, these fits do not support that hypothesis.

The BB temperatures cover a similar range in both outbursts, starting off cool, around 20–30 eV, before increasing. The inclusion of the edges leads to a larger rise in fitted temperature. The 2021 data show more variability in the BB parameters at the earliest times (i.e. before about day 30), when the SSS is only weakly present; this is particularly the case where absorption edges are included in the fit, which is likely a symptom of overfitting the data.

A large difference between the data sets is the excursion in BB kT around day 40 in 2006 (with and without absorption edges), where these data are better fitted with a temperature about 20–40 eV higher than observations shortly before or after this time (a bigger discrepancy when the edges are included). $N_{\rm H, wind}$ is correspondingly lower during this interval. The fitted temperature and column density are, of course, correlated to some level, due to the modest spectral resolution of the XRT at these energies. Forcing a higher $N_{\rm H, wind}$ causes the BB temperature to decrease (or vice versa); these forced fits are statistically worse, though. These observations with higher BB kT occurred during the time of large-scale flux variability – something that was not seen to such an extent in 2021, so it is perhaps unsurprising that the same variation in temperature/absorption is not found following the latest eruption.

Osborne et al. (2011) describe a rather different evolution of the SSS temperature compared with the reanalysis of those same 2006 data herein, finding significant changes in kT throughout the early flux variability phase, which then settled at the highest value reached. This may be caused by the differences in how the absorption is modelled. As noted above, Osborne et al. (2011) constrain $N_{\rm H, wind}$ to follow a power law of $t^{-0.5}$ cm^{-2} after the first detection of the SSS emission (based on work in Bode et al. 2006). In our re-analysis, where $N_{\rm H, wind}$ is freely fitted, we initially find a more variable column, particularly during the chaotic start to the SSS phase (though note mention of $N_{\rm H, wind}$–BB kT degeneracies above). However, after $\sim$day 50, the fit results for the 2006 data set are not inconsistent with a power-law decline in $N_{\rm H, wind}$ of index 0.5, although there is still significant scatter. The estimate of the range of the absorbing column in 2021 is very similar to that in 2006 until around day 60, when it decreases more significantly.

Around day 53 in 2021, there seems to be a brief dip in the effective BB radius, and an upward step in the temperature, corresponding to
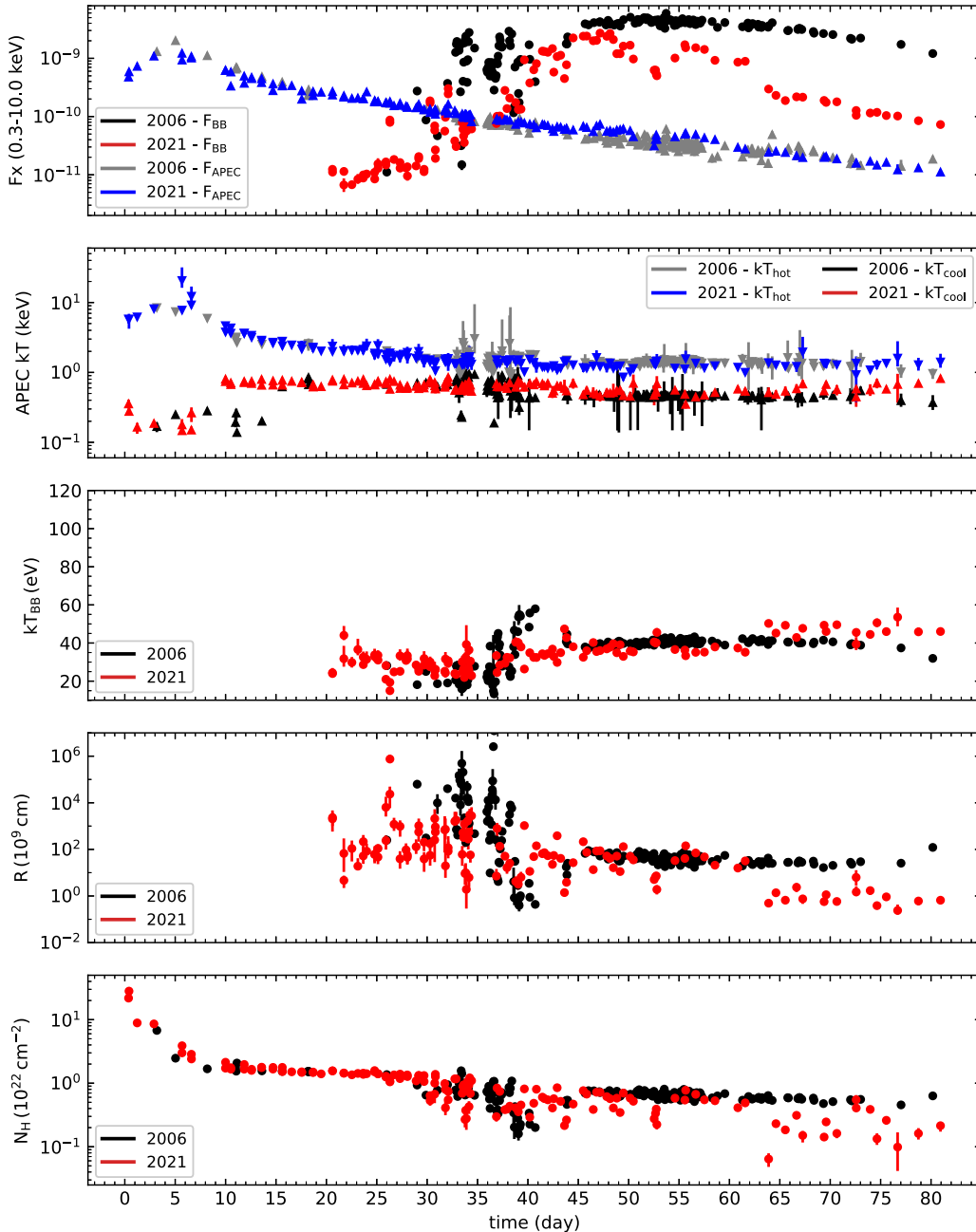
Figure 11. Results from fitting the spectra from 2006 and 2021 with a simple BB to model the soft emission, together with two optically thin APEC components. The top panel shows the observed 0.3–10 keV fluxes from the BB and APEC components (in units of erg cm^{-2} s^{-1}). The second panel shows the evolution of the APEC component temperatures, while the third panel shows the same for the BB. The fourth panel shows the emission radius for the BB component, and the bottom panel shows how the absorbing column $N_{\rm H, wind}$ (in excess of the Galactic ISM value) evolves with time. 2006 data are plotted in monochrome, while 2021 are in blue (hotter APEC parameters) and red (cooler APEC and all other parameters). Note that the ordinate scales are the same in each panel as in Fig. 12, for ease of comparison. See text for more details of the models.

the temporary drop in observed soft flux at that time. About a week later, after day 60, the 2021 BB temperatures become consistently slightly hotter, with a notable decrease in the corresponding emitting radius compared with 2006. It is not unexpected that, as the WD runs out of fuel, the bloated outer layers begin to shrink and, consequently, the BB temperature rises (e.g. Macdonald, Fujimoto & Truran 1985; Krautter et al. 1996; Shore, Starrfield & Sonneborn 1996b). However, from our fit results, the drop in radius is only obvious in 2021 over the time frame considered (i.e. before day 86). This could be an

indication that the nuclear burning phase ended earlier in 2021 – though see discussion in Section 6.3. The geometry of nova systems post-eruption is not always clear, though, and the WD may remain bloated long after the end of the eruption (e.g. Mason et al. 2021).

In Fig. 13, we show the bolometric luminosities estimated from the BB fits to the data after day 40, for both the zero and multiple edge models, in 2006 and 2021. The inclusion of (significant) absorption edges decreases the estimated luminosities overall, in both years. The low 0.3–10 keV flux measurements seen in 2021, particularly after
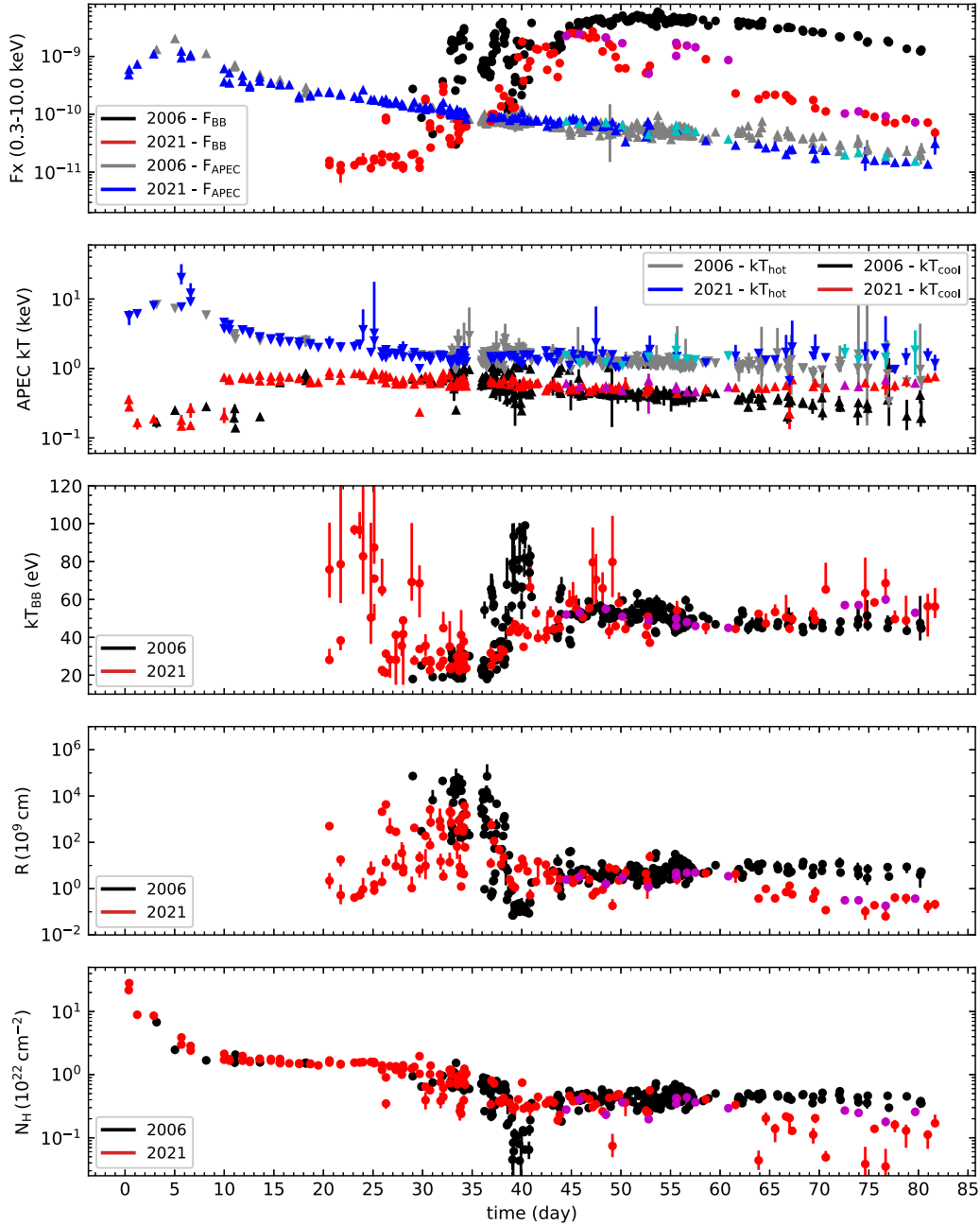
Figure 12. As for Fig. 11, but including four absorption edges as well. 2006 data are plotted in monochrome, while 2021 are in blue/cyan (hotter APEC parameters) and red/magenta. (Cooler APEC and all other parameters: red where BB kT was free to vary, magenta where that temperature was constrained. The APEC temperatures plotted in magenta and cyan correspond to the magenta BB bins, likewise for the radius and N_H.) Note that the ordinate scales are the same in each panel as in Fig. 11, for ease of comparison. See text for more details of the models.

day 60, clearly correspond to much lower bolometric luminosities. This is also the time frame over which the BB radius decreases (consistently) in 2021. It is well known that BB models can overestimate luminosities (e.g. Krautter et al. 1996), so the high peak values of $100-1000 L_{Edd}$ shown in Fig. 13 should not be taken as physically realistic, and only the comparative trends considered.

The optical [Fe X] 6375 Å coronal line (ionization energy of 235 eV) is often considered to be a tracer for the SSS phase, since it acts as a good indicator of photoionization from a hot WD (Krautter & Williams 1989). While more energetic photons from the

shocked ejecta will also be able to excite the [Fe X] emission line, the behaviour of the line is much more reminiscent of the SSS evolution.

The evolution of the optical [Fe X] line flux is therefore presented in Fig. 14, with the X-ray light curves for comparison. In 2021, the last non-detection of the line occurred on day 23.10, with the first positive detection occurring on day 25.10. In an effort to compare with the previous 2006 outburst, we have also measured the flux of [Fe X] on four of the eight spectra presented by Munari et al. (2007) – those for which an accurate absolute flux calibration is available – and these results for 2006 are overplotted as blue squares in Fig. 14.

Table 1. Fits to the XRT spectra before (model consisting of two absorbed APEC components) and during (including an additional BB) the SSS phases in 2006 and 2021, as plotted in Figs 11 and 12. The first column lists the mid-point of the spectrum in days since the optical peak of the eruption, while the second column provides the excess absorption. Columns 3–5 list the temperatures of the BB and APEC components, while columns 6 and 7 show the observed flux over 0.3–10 keV for the BB and combined APEC components, respectively. The final column gives the Cash statistic and number of degrees of freedom (dof). The full version of this table is available online.

| T_{mid} (d)	$N_{\mathrm{H, wind}}$ (10^{22} cm^{-2})	kT_{BB} (eV)	APEC kT_{cool} (keV)	APEC kT_{hot} (keV)	BB flux (erg cm^{-2} s^{-1})	APEC flux (erg cm^{-2} s^{-1})	C-stat/dof
2006 eruption							
3.178	$6.77^{+0.40}_{-0.38}$	–	$0.168^{+0.023}_{-0.028}$	$8.449^{+0.637}_{-0.576}$	–	$1.30^{+0.02}_{-0.02} \times 10^{-9}$	903.6/799
5.033	$2.47^{+0.10}_{-0.09}$	–	$0.248^{+0.017}_{-0.024}$	$7.407^{+0.312}_{-0.310}$	–	$2.01^{+0.02}_{-0.02} \times 10^{-9}$	1175.1/854
8.183	$1.68^{+0.10}_{-0.10}$	–	$0.280^{+0.017}_{-0.017}$	$5.964^{+0.335}_{-0.268}$	–	$1.11^{+0.01}_{-0.01} \times 10^{-9}$	1007.5/781
10.99	$1.75^{+0.16}_{-0.20}$	–	$0.192^{+0.041}_{-0.028}$	$2.976^{+0.199}_{-0.165}$	–	$6.50^{+0.17}_{-0.18} \times 10^{-10}$	655.4/602
11.057	$1.55^{+0.19}_{-0.20}$	–	$0.263^{+0.039}_{-0.054}$	$3.208^{+0.294}_{-0.251}$	–	$6.97^{+0.23}_{-0.21} \times 10^{-10}$	563.1/574
11.124	$2.07^{+0.02}_{-0.08}$	–	$0.138^{+0.011}_{-0.007}$	$2.688^{+0.093}_{-0.082}$	–	$6.79^{+0.19}_{-0.12} \times 10^{-10}$	574.4/585
13.605	$1.56^{+0.10}_{-0.11}$	–	$0.200^{+0.019}_{-0.012}$	$2.535^{+0.101}_{-0.074}$	–	$4.82^{+0.08}_{-0.08} \times 10^{-10}$	749.4/659
15.616	$1.54^{+0.06}_{-0.06}$	–	$0.621^{+0.020}_{-0.058}$	$2.782^{+0.109}_{-0.096}$	–	$3.89^{+0.06}_{-0.06} \times 10^{-10}$	890.9/639
18.176	$1.54^{+0.11}_{-0.13}$	–	$0.800^{+0.044}_{-0.038}$	$2.533^{+0.256}_{-0.203}$	–	$2.31^{+0.09}_{-0.04} \times 10^{-10}$	408.5/437
18.229	$1.50^{+0.16}_{-0.18}$	–	$0.844^{+0.064}_{-0.070}$	$2.427^{+0.630}_{-0.380}$	–	$2.29^{+0.08}_{-0.10} \times 10^{-10}$	257.0/311
18.239	$1.54^{+0.11}_{-0.13}$	–	$0.665^{+0.056}_{-0.051}$	$2.597^{+0.289}_{-0.212}$	–	$2.89^{+0.10}_{-0.10} \times 10^{-10}$	447.0/461
25.998	$1.37^{+0.04}_{-0.05}$	$28.1^{+1.6}_{-0.8}$	$0.672^{+0.040}_{-0.015}$	$2.047^{+0.156}_{-0.127}$	$1.11^{+0.06}_{-0.06} \times 10^{-11}$	$1.70^{+0.03}_{-0.03} \times 10^{-10}$	665.9/499
29.01	$0.94^{+0.03}_{-0.02}$	$18.1^{+0.3}_{-0.4}$	$0.701^{+0.015}_{-0.015}$	$1.569^{+0.047}_{-0.059}$	$2.74^{+0.02}_{-0.02} \times 10^{-10}$	$1.48^{+0.02}_{-0.02} \times 10^{-10}$	715.8/467
29.886	$0.65^{+0.03}_{-0.04}$	$25.1^{+1.0}_{-0.6}$	$0.707^{+0.038}_{-0.016}$	$1.602^{+0.056}_{-0.038}$	$8.73^{+0.13}_{-0.13} \times 10^{-11}$	$1.30^{+0.02}_{-0.02} \times 10^{-10}$	836.0/432
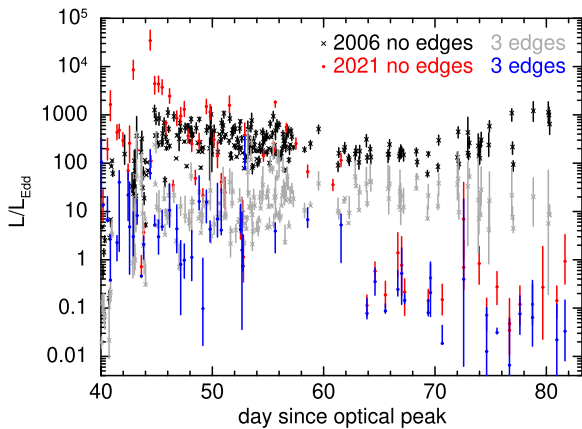
Figure 13. Bolometric luminosity estimates from the BB fits for the 2006 (black/grey) and 2021 (red/blue) data, without and with absorption edges. Whether or not the edges are included, the 2021 data are systematically less luminous than the 2006 data after day 60. The luminosity is plotted in terms of the Eddington value for a 1.4 M$_\odot$ WD (1.76×10^{38} erg s^{-1}), commensurate with the upper limit on the WD mass in Mikołajewska & Shara (2017).

The overall shape and duration of the [Fe X] curve is more similar to the X-ray evolution seen in 2006 than in 2021.

5 1985 ERUPTION

Following the 1985 eruption, the *European X-ray Observatory Satellite* (*EXOSAT*) observed RS Oph six times between days 54 and 250 after the peak of the optical emission, the first time the nova had been observed in X-rays (Mason et al. 1987). Four of these observations lie within the post-outburst time frame we are considering in this paper. We extracted the count rates from the High Energy Astrophysics Science Archive Research Center (HEASARC)
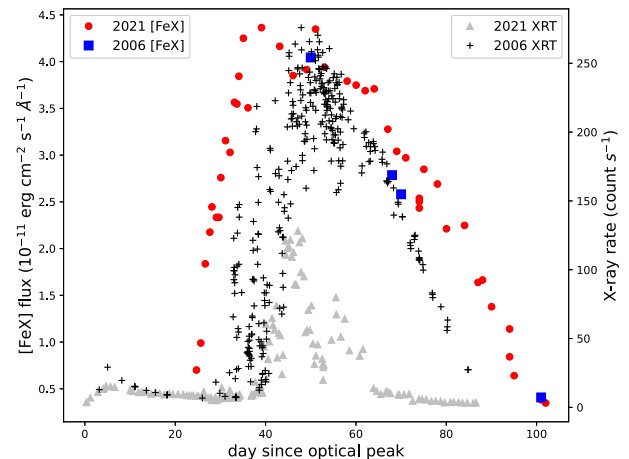

Figure 14. The evolution of the [Fe X] flux in 2021 and 2006 (red circles and blue squares; left-hand scale), compared with the corresponding 0.3–10 keV X-ray light curves (grey triangles and black pluses; right-hand scale).

data base,[10] and converted the Low Energy Imaging Telescope with the Lexan 3000 filter (LE-LX3)[11] measurements (0.05–2 keV) to *Swift* 0.3–1 keV count rates using Portable, Interactive Multi-Mission Simulator (PIMMS).[12] This gave an approximate conversion of 1 count s^{-1} with the LE-LX3 corresponding to ~13–17 count s^{-1} in XRT-WT (grade 0) over 0.3–1 keV; this range was estimated by taking the BB and N_{H} values from the fits closest in time to each

[10] https://heasarc.gsfc.nasa.gov/cgi-bin/W3Browse/w3browse.pl
[11] The Medium Energy proportional counter (ME; 1.2–50 keV) was also used, but the source was only detected during the first three observations.
[12] https://heasarc.gsfc.nasa.gov/cgi-bin/Tools/w3pimms/w3pimms.pl
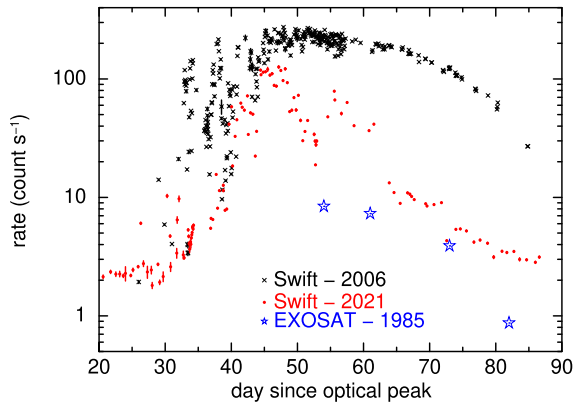
Figure 15. Comparison of the *EXOSAT* LE-LX3 observations following the 1985 eruption of RS Oph with the *Swift* light curves between 2006 and 2021. The *EXOSAT* measurements have been converted to *Swift*-equivalent 0.3–1 keV count rates using WebPIMMS.

EXOSAT post-eruption day from both 2006 and 2021.[13] Mason et al. (1987) attempted to fit the *EXOSAT* ME data over ∼1.5–5.5 keV. They found that the spectrum shows a strong rise at the soft-energy end, indicating the emission was likely supersoft, as assumed for this conversion.

Fig. 15 shows these converted *EXOSAT* measurements (using the mean conversion of 1 *EXOSAT*-LE count s^{-1} = 15 *Swift*-XRT counts s^{-1}) with respect to the *Swift* light curves from 2006 and 2021, indicating that the soft X-ray emission in 1985 was even fainter than in 2021. However, the 1985 data drop off rapidly after day 60–70, more like the 2006 eruption than the 2021 one. Interestingly, the 1985 and 2006 eruptions occurred at about the same binary phase, while 2021 was ∼180° different. Note that the RS Oph eruption prior to 1985 occurred in 1967, so the 1985 eruption followed a quiescent interval of 18 yr.

The X-rays detected with the limited *EXOSAT* observations were previously interpreted to be shock emission (Mason et al. 1987), although O'Brien, Bode & Kahn (1992) suggested that a better solution might be that the shock in the RG wind provides the higher energy X-ray emission whilst most of the low-energy flux is due to the WD remnant. With the more detailed observations from *Swift*, we can state that the majority of these X-rays were most likely supersoft photons from the surface nuclear burning as it switched off (as also concluded by Ness et al. 2007b). Indeed, while Mason et al. (1987) interpreted the earlier observations (including all those presented here in Fig. 15) as shock-heated thermal emission, they ascribe the last detection around day 250 to residual nuclear burning on the WD surface.

6 DISCUSSION

With a mean recurrence time-scale of 15 yr, RS Oph is the first Galactic recurrent nova for which more than one eruption has been monitored by *Swift*. The quiescent interval preceding the 2021 eruption was 15.5 yr, close to this mean value; the 21 yr gap between 1985 and 2006, however, is around 35 per cent longer than the average. In this paper, we perform a detailed comparison of the

---

[13]We note that Ness et al. (2007b) scaled the *EXOSAT* data by eye to reproduce the XRT count rate on day 55 after the 2006 eruption, leading to a very different comparison.

XRT data collected during the first ∼86 days of these eruptions, to investigate how similar – or different – the events were.

The most obvious difference that requires explanation is the clearly brighter observed X-ray emission in 2006 compared with 2021 (and 1985). Here we summarize all the salient points.

Similarities

(i) The optical light curves in 2006 and 2021 are almost identical. This strongly suggests that the WD mass, ejecta mass, velocity distribution, and geometry are close to constant, since these are the parameters that affect the optical evolution (e.g. Shore 2012; Chomiuk, Metzger & Shen 2021, and references therein).

(ii) Despite limited data from 2006, the evolution of the [Fe X] coronal emission appears to be approximately the same following both eruptions.

(iii) The harder X-ray emission (dominating >1 keV) produced by shock interactions between the nova ejecta and the RG wind was similar, in terms of both brightness and temperature evolution, throughout the majority of the interval considered. This, like the identical optical light curves, implies the ejecta parameters are similar, as well as the gross properties of the RG wind density structure close in to the system.

(iv) The SSS emission became visible around the same time (day 20–26), and the final decline started around day 60 after each eruption.

(v) The magnitude and temporal evolution of the wind absorbing column (in excess of the Galactic value) was typically similar until day 60, although the 2006 data show more variation during the end of the high-amplitude flux changes (around day 40).

(vi) The parametrization of the SSS with a BB mainly provided similar temperatures between the two eruptions, with or without the inclusion of absorption edges.

(vii) A QPO was identified in both 2006 and 2021, with a consistent mean period of ∼35 s. The modulation fraction was also similar during both eruptions.

Differences

(i) The measured count rate at the beginning of the SSS phase in 2006 was more variable than in 2021.

(ii) The count rate peaks and troughs occurred at different times following each eruption.

(iii) The SSS emission in 2006 was brighter than in 2021, peaking at more than double the count rate over 0.3–1 keV. The integrated number of soft X-ray counts is ∼4–5 times larger in 2006 than 2021.

(iv) The 2006 eruption occurred after an intereruption gap of 21 yr, about 35 per cent longer than the average recurrence time. The 15.5 yr quiescent interval that ended in 2021 is almost exactly the average duration.

(v) In 2006, the SSS emission plateaued around a peak count rate between ∼days 45 and 60, before a monotonic decline set in. The 2021 soft emission stayed at peak brightness from around days 45–48, then faded by a factor of about 5 over the next 5 d, followed by a brief rebrightening before a final fading trend set in around day 60.

(vi) After day 76, the rate of decline of the 2006 soft emission was more than twice as rapid as at the corresponding time in 2021.

(vii) As noted above, the range of BB temperatures was similar during both SSS phases. However, the 2006 spectra show a more rapid increase in temperature, then staying approximately constant until day 70. The 2021 temperature increase is gradual, becoming systematically hotter than the corresponding 2006 data after day 60; this is more obvious with the simple BB fits with no edges included,

but the trend is still there with the edges. The 2006 data are also noticeably hotter for an interval around day 40.

(viii) The 2006 spectra show more signs of absorption features, with the 2021 spectra appearing much smoother; those fits are therefore not significantly improved by the inclusion of ionized absorption edges, whereas the 2006 data are.

(ix) After ∼day 60, the radius of the emitting region in 2006 is consistently higher than in 2021, caused by the 2021 radius dropping, while the 2006 measurement stays approximately constant. This is the case with or without absorption edges. There is also a brief decrease in the 2021 BB radius around day 53, corresponding to the temporary drop in soft flux, though this is not clearly seen when edges are included.

(x) $N_{\rm H, wind}$ is also lower after ∼day 60 in 2021, though very similar in both 2006 and 2021 at earlier times.

(xi) After day 60, the apparent bolometric SSS luminosity in 2006 was much higher than in 2021.

The results of the spectral fitting (Figs 11 and 12) imply the higher SSS count rate and luminosity in 2006, particularly after day 60, were due to a larger effective emitting surface compared with the recent 2021 eruption. There is no indication that the lower count rates in 2021 are caused by higher absorption, though we return to this possibility in Section 6.4. From the numbered points above, it is notable that many of the differences between the 2021 and 2006 X-ray spectral evolution results occur after day 60 – i.e. the time both X-ray light curves showed a final monotonic fading, signifying the end of the nuclear burning. At earlier times, during the onset of the SSS phase, there is also a significant difference in the level of soft X-ray variability seen.

6.1 Differences in SSS related to quiescent interval?

While the *EXOSAT* data set is much smaller than those of *Swift*, it is clear that there were very significant differences in the soft X-ray emission between the three RS Oph eruptions, which followed quiescent intervals of around 18, 21, and 15.5 yr, respectively. M31N 2008-12a, the yearly recurrent nova in the Andromeda galaxy, has been observed by *Swift* during every eruption since 2012. For the first 4 yr of observations, the X-ray light curves of M31N 2008-12a were very similar; the 2016 event was a surprise, though, showing a delayed start leading to a shorter and less luminous SSS phase (Henze et al. 2018). The optical light curve, however, showed little variation from outburst to outburst, which is also the behaviour witnessed for the RS Oph optical data. The intereruption time for M31N 2008-12a varies by ∼15 per cent, year-on-year (Darnley et al. 2016), while still (except for 2016) showing a consistent SSS phase. Henze et al. (2018) suggest that the differences seen in 2016 (delayed eruption – i.e. longer quiescent interval; earlier decline in the SSS emission) could be explained by a lower accretion rate, $\dot{M}_{\rm acc}$, between outbursts. This would have led to a lower mass disc, which was thus more disrupted by the nova explosion than the discs usually formed. A more thoroughly disrupted disc in turn leads to a longer delay before effective accretion restarts, hence shortening the SSS phase in this system. In the current case of RS Oph, the 2006–2021 quiescent interval was *shorter* than 1985–2006; however, the 2021 SSS was none the less fainter. Thus the behaviour of RS Oph does not replicate the longer quiescent interval/fainter SSS situation seen in M31N 2008-12a. There is also no strong sign of the mean accretion rate being different during the RS Oph intereruption intervals (see Section 6.2.1 below).

6.2 Quiescence

6.2.1 Accretion rate and luminosity

Modelling by Prialnik et al. (1982) suggests that different accretion rates, $\dot{M}_{\rm acc}$, can lead to different accreted masses being required to initiate a TNR. If $\dot{M}_{\rm acc}$ is higher, both the accretion energy, and the rate at which the compressional energy is released, increases. This causes the temperature on the WD surface to increase more rapidly for a given amount of accreted mass, meaning that less mass needs to be accreted before the environment becomes hot enough to initiate a TNR. In such a situation (i.e. higher $\dot{M}_{\rm acc}$ over a shorter interval), we would expect a weaker nova explosion, with less material available to burn. Thus, if the accretion rate were higher during the 2006–2021 interval compared with 1985–2006, we could expect a less extreme eruption, with a shorter/weaker SSS phase in 2021.

RS Oph was intermittently observed by *Swift* between the 2006 and 2021 eruptions. Considering the 31.3 ks of data collected between 2009 August and 2020 July (days 1284–5269 after the 2006 eruption, during which time the X-ray count rate remained close to constant), the spectrum can be approximated with an optically thin model, with $kT = 1.0 \pm 0.2$ keV (C-stat/dof = 55/69). This spectrum has a 0.3–10 keV count rate of 4.0×10^{-3} counts s^{-1} (well below the level observed just before the Sun constraint in 2021), which corresponds to a bolometric (unabsorbed) luminosity of ∼6×10^{31} erg s^{-1}. Such a measurement is in the same range as the quiescent luminosity determined from the *ROentgen SATellite* (*ROSAT*) observations between the 1985 and 2006 outbursts (Orio 1993; see also estimates in Mukai 2008). This suggests a consistent mass accretion rate during both quiescent periods – though is by no means definitive, given the small number of observations being compared.

A comparison of the AAVSO optical light curves from 1985–2006 and 2006–2021 also shows no large differences during the intereruption periods. The optical magnitude does appear to brighten by up to a magnitude during the ∼5 yr before each eruption, though. The mean quiescent visual magnitudes from these data sets are 11.3 (1985–2006) and 11.1 (2006–2021), each with a standard deviation of ∼0.4. However, in general the disc luminosity is proportional to $\dot{M}_{\rm acc}$. A ∼35 per cent longer recurrence time up to 2006 would then suggest $\dot{M}_{\rm acc}$, and hence the disc luminosity, are ∼35 per cent lower, which equates to a change in magnitude of about 0.3. This would likely be swamped by the optical light from the donor star, so measuring such a change in the accretion rate in this manner would be tricky. Observations in the near-UV band should be more informative.

Osborne et al. (2011) comment that this estimated quiescent X-ray luminosity is orders of magnitude lower than the expected interoutburst accretion value of ∼few × 10^{36} erg s^{-1}. Mukai (2008) consider methods through which the expected quiescent X-ray emission could be suppressed. They concluded it unlikely that absorption could be the sole cause, since an unfeasibly high column would be required to hide emission over 2–10 keV. If the boundary layer between the accretion disc and WD surface were optically thick, then softer X-rays would be emitted that could more easily be strongly absorbed, although an optically thick boundary layer is not expected in quiescence. Nelson et al. (2011) analyse observations obtained by *Chandra* and *XMM–Newton* 537–744 d after the 2006 eruption, finding the X-ray spectra can be modelled with a two-component plasma model (as we see here, underlying the SSS). Using this model, they determine an intrinsic accretion luminosity of 1–2 × 10^{35} erg s^{-1} from the boundary layer. They find that a

combination of a complex (partial-covering) absorber and optically thick emission from the boundary layer could indeed account for the apparently low quiescent luminosity measured. The X-ray flux at this time was still apparently following a power-law decline that started around day 100 post the 2006 eruption (Osborne et al. 2011; Page et al. 2020), although considering the later light curve as well, there were signs that the decline might have been ending; thus the interpretation of the flux as accretion powered may not be secure.

To summarize: the measured X-ray emission during quiescence provides no strong evidence for a difference in accretion rate between 1985–2006 and 2006–2021. A simple estimate of the accretion luminosities over these two quiescent intervals gives values orders of magnitude lower than expected, though this conflict might possibly be resolved if there is complex absorption in the system.

6.2.2 Accreted mass

The accreted mass required to trigger the TNR in RS Oph is $\approx 4.4 \times 10^{-6}$ M$_{\odot}$ (Osborne et al. 2011, following Truran & Livio 1986), and a steady mass transfer over an interval of 21 yr will obviously lead to a greater build-up of material than over only 15.5 yr. Although having less accreted material to burn might account for a fainter, or shorter lived, SSS phase in 2021, it fails to explain why the nova did not erupt 5.5 yr before the 2006 event, when that same amount of material had been built up. Neither does it explain the fact that the optical evolution is identical, nor that the turn-on time of the SSS phase is very similar. As discussed above, Prialnik et al. (1982) show that a higher accretion rates might lead to lower accreted masses being needed to trigger a TNR, but there is no strong evidence that $\dot{M}_{acc}$ has varied significantly between the recent eruptions of RS Oph.

Osborne et al. (2011) find that the mass burnt/ejected during the 2006 nova is likely only a few per cent of the accreted envelope, and that the WD in the RS Oph system is therefore gaining mass with time (see also Hachisu, Kato & Luna 2007). This mass gain during a single eruption cycle is, however, relatively small, and will not noticeably change the expected recurrence time.

6.3 [Fe X]

As noted above, the [Fe X] line is thought to mirror the evolution of the central source luminosity, and is therefore suggested to match up with the SSS emission seen in the X-ray band (see discussion in Schwarz et al. 2011). From Section 3.1, the first hint of a soft excess in the 2021 X-ray spectrum was day 20.6, becoming significantly stronger from day 26.3. A monotonic decline in the X-ray flux set in after about day 60. These timings are loosely replicated by the changes in the [Fe X] flux.

While there are many fewer measurements available from 2006 than 2021, the [Fe X] fluxes in Fig. 14 align fairly well following the two eruptions. The 2021 [Fe X] curve is much smoother than the soft X-ray emission we measured in 2021 (see also Fig. 3), and more reminiscent of the underlying shape of the 2006 X-ray light curve. The [Fe X] emission is believed to come from the body of the ejecta photoionized by the WD, and should generally be insensitive to occulting blobs of matter that would absorb the soft X-rays. The [Fe X] evolution shown in Fig. 14 suggests that the nuclear burning was again relatively steady throughout the 2021 eruption, and likely very similar in duration in both 2006 and 2021. This therefore does not seem to agree with the inferred decrease in the BB radius in 2021 corresponding to an earlier end to the nuclear burning, but rather suggests the SSS phase was the same both years.

Note that the recombination time-scale of [Fe X] in this density environment will likely be a day or less (Munari & Valisa 2021b, Munari et al., in preparation), so cannot cause the differences seen.

Fig. 5 of Munari & Valisa (2022) shows that the fluxes of the coronal lines [Fe X], [Fe XI], and [Fe XIV] all begin to decline from their plateau phase around day 87 (seen as a steepening in the decay in Fig. 14, where we show the [Fe X] flux in linear space), which strongly suggests the same power source (presumably the nuclear burning) switched off for them simultaneously, at which point the WD would start to cool. The shock breakout at the edge of the RG wind could also have an effect, however (Shore et al. 1996a).

6.4 Absorption

Looking solely at Fig. 3, one's first assumption might be that the lower soft flux in 2021 is due to greater absorption than in 2006. Excluding the interval of high-amplitude flux variability between days 30 and 40 (which may itself be caused by clumpy ejecta; Osborne et al. 2011), the 2021 observed flux is systematically much lower than in 2006 after day 45. This drop would require a large absorbing structure moving into view at this time, given that the 2021 flux is significantly lower for at least 40 d (about 10 per cent of the binary orbit). If absorption were the cause of the 1985 X-rays being fainter, then the absorbing structure would need to be non-permanent, since the 1985 and 2006 eruptions occurred at similar orbital phases.

The simulations by Booth, Mohamed & Podsiadlowski (2016) show a spiral accretion wake built up during the quiescent mass transfer, potentially positioned along our line of sight to the WD during the time of the 2021 eruption (around phase 0.72). In comparison, the 2006 nova took place at phase 0.26, where the simulations show a lower density. The 1985 eruption occurred around phase 0.32, closer to the 2006 viewing angle than 2021, but the X-ray emission measured in 1985 was even fainter than in 2021. Booth et al. (2016) do find their simulated structure to be clumpy, though, that could possibly account for this. Modelling by Orlando et al. (2009), Drake et al. (2009), and Walder et al. (2008) also shows distinctly aspherical mass loss in the binary system, all indicating the absorption seen will likely depend on the phase of the orbit during the observations.

Shore & Aufdenberg (1993) and Shore et al. (1996a) investigated the UV spectra of recurrent novae, including RS Oph following the 1985 outburst, finding differential absorption along the line of sight, and that the orbital modulation of the intensity of the ionizing source by the circumstellar medium can affect the strength of the emission lines. That is, no change in the photoionization source itself was needed to cause the spectral changes seen; rather, an aspect change in the line-of-sight opacity could explain the differences.

Considering the more recent eruptions of RS Oph, work by Azzollini (2021) and Azzollini et al. (in preparation) finds that, although the optical photometric light curves between 2006 and 2021 are the same, individual line fluxes (measured from the UVOT UV grism spectra) in 2021 are a factor of ~10–100 below the corresponding values in 2006. There is a chromatic dependence to this, with shorter wavelength lines showing larger decrements; this may be due to Rayleigh scattering – the interaction of photons with bound electrons. That is, the neutral hydrogen, distributed around the emitting source, scatters the optical and UV line photons out of our view. Thus, if, in 2006, our line of sight passed through a more ionized region (e.g. if the ionization of the wind is variable at different orbital phases), less Rayleigh scattering would occur, and higher line fluxes would be measured – which is indeed the case.

Whatever the simulations and modelling potentially show, however, the results from our spectral fitting do not obviously support significant differences in absorption. Figs 11 and 12 show that the fitted $N_{H, wind}$ is largely consistent between the two eruptions, with the fainter 2021 data actually showing a *lower* column after day 60. This drop in $N_{H, wind}$ after day 60 in 2021 could conceivably be related to the edge of the RG wind, established since the 2006 eruption. With the shorter recurrence interval, the wind has only had 15.5 yr of traveltime, rather than the 21 yr prior to 2006. In 2006, this wind shock breakout time was found to occur around day 80 (Anupama 2008).

We considered a small sample of spectra where we have data on the same day post-eruption in both 2006 and 2021. In each case, the best-fitting 2006 model was applied to the corresponding 2021 spectrum, with only the absorbing column density and edge depths allowed to vary. This assumes a simplified model, whereby the underlying SSS and shock emission were exactly the same at corresponding days in both 2006 and 2021, and the only difference was the intervening column. The resulting fits were statistically much worse (Δ C-stat $\sim 100–700$), indicating these models are not acceptable, and it is unlikely we are seeing identical nuclear burning (temperature and strength), with only a change in $N_{H, wind}$. The fit results in Figs 11 and 12 also imply that the emitting radius was smaller after around day 60 in 2021, though it is not clear whether this is caused by the ending of nuclear burning, or some other effect.

The absorption fitted to the X-ray spectra presented here has been assumed to be neutral. If, instead, there is an ionized component as suggested by the optical/UV analysis, or the abundances are non-solar, this could affect the results. Indeed, the ionized He- and H-like nitrogen and oxygen absorption edges are notably more significant in the 2006 X-ray spectral fits, which could be a sign of the differing ionization states observed.

In summary, we find that the lower soft X-ray flux seen in 2021 compared with 2006 cannot readily be explained by an increase in simple neutral absorption. The investigation by Nelson et al. (2011) of post-eruption RS Oph data suggests that the absorbing column(s) may be more complex, however. We reiterate that the inclination angle of the RS Oph system is estimated to be in the range $30°–52°$, which places constraints on the amount of absorption to which the accretion disc could lead.

A paper analysing the much higher signal-to-noise ratio *NICER* spectra is in preparation (Orio et al. in preparation) and this may shed more light on the spectral complexities.

6.5 A combination nova?

The outbursts of RS Oph have been suggested to be due to a dwarf nova (DN) disc instability, in which a burst of enhanced mass accretion triggers the outburst, rather than a TNR due to steady accretion during quiescence (King & Pringle 2009), although a TNR-driven outburst is preferred (see summary by O'Brien et al. 1992, for example).

A related suggestion is that RS Oph is a 'combination nova' (Sokoloski et al. 2006). These are sources that show both dwarf and classical nova characteristics: eruptions in these systems start off as an accretion disc instability (as happens in DNe), leading to sufficient material being accreted to trigger the thermonuclear burning and mass ejection expected from a 'normal' nova. Alexander et al. (2011) suggest that the outbursts in RS Oph could be powered by an accretion dump due to a single-disc instability, while the model by Bollimpalli, Hameury & Lasota (2018) requires multiple DN events to provide the fuel more slowly to cause a TNR over the recurrence time observed. These disc instability events should be detectable

in X-rays, yet no such events have been reported. However, DN outbursts can be faint, and RS Oph is more distant than most DNe (e.g. Patterson 2011). We also note that the model by Bollimpalli et al. (2018) requires the WD to have a significant magnetic field, as we discuss for the QPO.

Could it therefore be that, in 2006, a disc instability led to a greater amount of material being dumped on to the WD than was the case in 2021 (or 1985)? This might explain the overall brighter SSS emission, and the fact that the integrated soft flux in 2006 was clearly larger than in 2021, and would sidestep the problem of the accretion rate apparently being approximately consistent over the 21 and 15.5 yr intereruption intervals (as discussed in Section 6.2.1). As noted in that section, there is some indication that during the final 5 yr before an eruption recurs, there is a slight brightening in the optical, possibly indicative of a change occurring in the accretion disc. Alternatively, it may suggest that energy from the incipient nuclear burning is reaching the surface some years before the actual thermonuclear runaway. Certainly this 5-yr brightening interval is longer than the expected duration of a DN outburst, which is in the range of 50–550 d in the Bollimpalli et al. (2018) models.

Closer in time to each eruption than this, Adamakis et al. (2011) identify a pre-outburst signal in the optical light curves of RS Oph, up to ∼450 d (one orbital period) before the subsequent nova, which they suggest may be caused by variable mass transfer. Bollimpalli et al. (2018) note that their combination nova model might explain this increase.

It is still unclear whether the RG in RS Oph fills its Roche lobe (though it seems likely it does; e.g. Brandi et al. 2009; Booth et al. 2016), or if accretion on to the WD occurs via stellar wind capture – or a combination of the two. While wind accretion does not *require* that an accretion disc exists, it also does not preclude one, and it is probable that there is a disc in the RS Oph system (see discussion by Wynn 2008). Such a structure would naturally be required for any form of disc instability to occur. Following the 2006 eruption, Worters et al. (2007) concluded that accretion was likely re-established between days 117 and 241, a minimum of several weeks after the intervals we are comparing in the current work, based on the reappearance of optical flickering. However, as Sokoloski et al. (2008) suggest, the earlier cessation of flickering noted by Zamanov et al. (2006) could just have been a sign of a change in the inner region of the accretion disc, rather than its complete destruction. Booth et al. (2016) also find that the disc survives the nova in most of their simulations. Somero, Hakala & Wynn (2017) comment that their high-resolution optical spectroscopy of RS Oph obtained 2–3 yr after the 2006 eruption did not show the double-peaked emission line profiles expected from an accretion disc, but note that this may be because the inclination of the system is too low.

A difficulty with the combination nova model, however, is the fact that the optical light curves are identical each time. The ejected mass (and hence the optical emission) following a nova explosion is very unlikely to be constant between eruptions spontaneously triggered in this manner.

6.6 QPO persistence

The fact that the QPO remains around 35 s during the distinctly different SSS phases following the two eruptions appears to be more consistent with a rotation explanation, rather than a pulsation mechanism (see Beardmore et al. 2008; Osborne et al. 2011; Ness et al. 2015; Wolf, Townsend & Bildsten 2018, for discussions about QPO provenance). However, this begs the question of why the SSS is not emitting smoothly over the entire surface of the WD, as might

typically be expected during a TNR. A possible explanation could be the presence of a magnetic field on the WD; this could manifest in a number of ways.

(i) The nuclear burning rate could be suppressed by the enhanced magnetic pressure at the poles, causing it to be lower. This is somewhat similar to the effect that leads to sunspots, whereby magnetic fields suppress the underlying convection, leading to cooler areas. Assuming the magnetic and rotational axes are misaligned, then this would lead to an observed flux modulation as the WD spins.

(ii) If accretion is occurring during the SSS phase, the stream could be magnetically funnelled towards the polar regions, causing a nuclear burning hotspot that would move in and out of view as the WD rotates. For examples of SSS with probable signs of magnetic field confinement, see King, Osborne & Schenker (2002), Aydi et al. (2018), and Drake et al. (2021). V1500 Cyg was a nova outburst on a highly magnetized WD, where a probable hotspot of enhanced nuclear burning occurred (Stockman, Schmidt & Lamb 1988). Shara (1982) discusses localized TNRs in more detail. If the luminosity is (super-)Eddington, however, accretion is not expected – at least, not fully spherical accretion.

In both of these possible cases, the majority of the SSS emission would come from the TNR spread over the full WD surface, with only small areas affected by magnetic fields leading to the detected modulation (see discussion in Aydi et al. 2018). While we are unaware of independent measurements of a magnetic field in RS Oph, coherent X-ray modulation is usually taken as sufficient evidence for this in accreting systems, and one is assumed in the model by Bollimpalli et al. (2018), as mentioned in Section 6.5.

A simple rotation effect would imply a fixed period, rather than one which varies, albeit slightly, as shown by the coherence measurements. (Although a low coherence can also indicate that the phase of the oscillation is changing, leading to a broader QPO signal, while the period remains fixed. This was seen during the 2006 eruption of RS Oph; Beardmore et al., in preparation.) Cal 83 (Crampton et al. 1987; van den Heuvel et al. 1992) is a persistent SSS: a WD accreting at a sufficiently high rate such that (quasi-)steady hydrogen burning occurs (Kahabka & van den Heuvel 1997). This source also shows a QPO (∼67 s), and Odendaal et al. (2014) suggested that the X-rays might originate from an extended atmosphere, only loosely coupled to the WD, so allowing differential, non-synchronous rotation (see also Warner & Woudt 2002).

6.7 Post-SSS emission

After several months in Sun constraint, late-time observations of RS Oph by *Swift* were obtained in 2022 February–April Fig. 16 shows that, at this time, the 2021 and 2006 eruption X-ray light curves and hardness ratios are in good agreement. The X-ray spectrum now shows little evidence for any residual SSS emission, so the underlying shock continuum continues to be the same almost 200 d post-eruption. As first suggested by Krautter et al. (1996) for V1974 Cyg, and later discussed by Osborne et al. (2011) for RS Oph in 2006, the X-rays seen during the decline from SSS peak may come from energy radiated as the remaining extended WD atmosphere undergoes gravitational contraction, and relaxes back on to the WD surface.

7 SUMMARY

RS Oph re-erupted in 2021, 15.5 yr after the previous nova event, and was monitored in detail by the *Swift* both times, the first Galactic
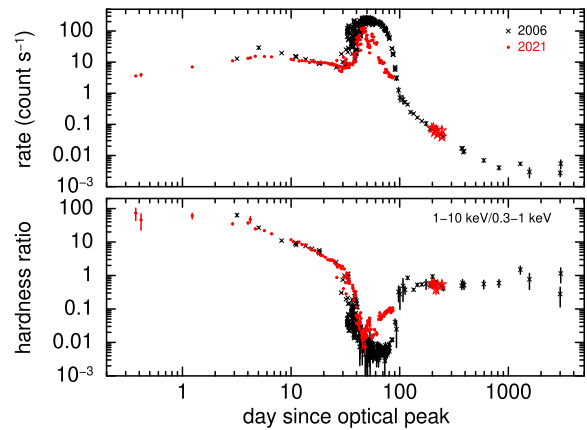
Figure 16. 0.3–10 keV light curves between 2006 and 2021, including the post-SSS data. The red stars highlight the post-Sun-constraint observations in 2022 February–April.

recurrent nova for which this has been possible. Lessons learnt from the first eruption led to the 2021 hard emission being monitored earlier and more frequently than in 2006, while the SSS phase was again followed closely. In this paper, we have compared the X-ray emission from these outbursts, together with another observed by *EXOSAT* in 1985.

The overall optical light curves were very similar in 2006 and 2021, suggesting the WD mass, ejecta mass, ejecta velocity distribution, and ejecta geometry have remained the same. The harder X-ray emission also indicates the ejecta and immediate circumstellar environment parameters have not changed significantly, since the shocks were very similar both times. The consistency in the 2006 and 2021 outbursts of the [Fe X] evolution is likely caused by a very similar duration, and luminosity, of nuclear burning.

The observed soft X-ray emission, however, was much brighter in 2006, with the ratio of the observed integrated soft X-ray counts being around 4–5 times higher than in 2021. This is a much larger factor than the difference in the quiescent intervals, so is unlikely to be due to a simple change in accreted mass. There is no clear sign of a change in accretion rate during the intereruption intervals, either.

While a higher absorbing column in 2021 would seem to be a simple explanation for the fainter X-rays detected, the fits to our spectra do not support this, with the measured $N_{\mathrm{H, wind}}$ being very similar in both 2006 and 2021 until day 60. A notable difference to come out of the spectral fitting, however, is a smaller BB emitting area in 2021 from around 2 months after the eruption. It is not immediately obvious whether this smaller radius is related to the expected shrinking of the bloated WD atmosphere as nuclear burning comes to an end, since the [Fe X] measurements imply the nuclear burning duration is similar for both eruptions. There is also a brief, earlier interval around day 53 in 2021, at the time when the observed soft flux decreased, where we also see a temporary drop in the effective BB radius.

Given that the differing optical and UV line fluxes may lean towards the ionization along our line of sight to RS Oph in 2006 being enhanced compared with 2021 (the orbital phases at the start of the two eruptions were almost 180° apart), it seems possible that our assumption of neutral absorption in the X-ray band may be an oversimplification.

In summary, while the optical magnitude, [Fe X], and hard X-ray light curves appear very similar following both 2006 and 2021 eruptions, the observed soft X-ray emission was found to be much

brighter in 2006 than in 2021 or 1985. We have explored some possible explanations for the difference in the supersoft phase, but our modelling of the *Swift*-XRT data does not provide any definitive conclusions. A reduced nuclear burning luminosity could explain the fainter X-rays in 2021 compared with 2006, although the [Fe X] line emission suggests a similar luminosity both times. If indeed the luminosity was consistent following the separate eruptions, then the SSS X-ray emission in the line of sight must be partly blocked, though the mechanism for this is unclear.

Looking ahead to the next RS Oph eruption, it is likely that the *Advanced Telescope for High Energy Astrophysics* (*Athena*) will have launched, and should be able to obtain high-resolution, high signal-to-noise ratio X-ray spectra. In general, UV and X-ray spectra in the late phase of the outburst will help to shed more light on the evolution of the nova ejecta; the proximity to the Sun during this latest event precluded this.

ACKNOWLEDGEMENTS

DATA AVAILABILITY

The X-ray data underlying this paper are available in the *Swift* archive at https://www.swift.ac.uk/swift_live/ and the HEASARC Browse archive at https://heasarc.gsfc.nasa.gov/cgi-bin/W3Browse /w3browse.pl.

REFERENCES

Acciari V. A. et al., 2022, Nat. Astron., preprint (arXiv:2202.07681)

Adamakis S., Eyres S. P. S., Sarkar A., Walsh R. W., 2011, MNRAS, 414, 2195

Alexander R. D., Wynn G. A., King A. R., Pringle J. E., 2011, MNRAS, 418, 2576

Anupama G. C., 2008, in Evans A., Bode M. F., O'Brien T. J., Darnley M. J., eds, ASP Conf. Ser. Vol. 401, RS Ophiuchi (2006) and the Recurrent Nova Phenomenon. Astron. Soc. Pac., San Francisco, p. 251

Arnaud K. A., 1996, in Jacoby G., Barnes J., eds, ASP Conf. Ser. Vol. 101, Astronomical Data Analysis Software and Systems V. Astron. Soc. Pac., San Francisco, p. 17

Aydi E. et al., 2018, MNRAS, 480, 572

Azzollini A., 2021, Master thesis, Univ. Pisa, Pisa, Italy

Bailer-Jones C. A. L., Rybizki J., Fouesneau M., Demleitner M., Andrae R., 2021, AJ, 161, 147

Barret D., Vaughan S., 2012, ApJ, 746, 131

Barthelmy S. D. et al., 2005, Space Sci. Rev., 120, 143

Beardmore A. P., Osborne J. P., Page K. L., Goad M. R., Bode M. F., Starrfield S., 2008, in Evans A., Bode M. F., O'Brien T. J., Darnley M. J., eds, ASP Conf. Ser. Vol. 401, RS Ophiuchi (2006) and the Recurrent Nova Phenomenon. Astron. Soc. Pac., San Francisco, p. 296

Beardmore A. P. et al., 2010, Astron. Telegram, 2423

Beardmore A. P., Osborne J. P., Page K. L., 2013, Astron. Telegram, 5573

Bode M. F., 1987, in Bode M. F., ed., RS Ophiuchi (1985) and the Recurrent Nova Phenomenon. VNU Science Press, Utrecht, p. 241

Bode M. F., Evans A., 2008, Classical Novae, 2nd edn. Cambridge Univ. Press, Cambridge

Bode M. F. et al., 2006, ApJ, 652, 629

Bode M. F., Harman D. J., O'Brien T. J., Bond H. E., Starrfield S., Darnley M. J., Evans A., Eyres S. P. S., 2007, ApJ, 665, L63

Bollimpalli D. A., Hameury J.-M., Lasota J.-P., 2018, MNRAS, 481, 5422

Booth R. A., Mohamed S., Podsiadlowski Ph., 2016, MNRAS, 457, 822

Brandi E., Quiroga C., Mikołajewska J., Ferrer O. E., García L. G., 2009, A&A, 497, 815

Burrows D. N. et al., 2005, Space Sci. Rev., 120, 165

Cash W., 1979, ApJ, 228, 939

Cheung C. C., Ciprini S., Johnson T. J., 2021a, Astron. Telegram, 14834

Cheung C. C., Johnson T. J., Mereu I., Ciprini S., Jean P., 2021b, Astron. Telegram, 14845

Cheung C. C. et al., 2022, ApJ, submitted

Chomiuk L., Metzger B. D., Shen K. J., 2021, ARA&A, 59, 48

Crampton D., Cowley A. P., Hutchings J. B., Schmidtke P. C., Thompson I. B., Liebert J., 1987, ApJ, 321, 745

Darnley M. J., 2021, PoS, GOLDEN2019, 44

Darnley M. J., Williams S. C., Bode M. F., Henze M., Ness J.-U., Shafter A. W., Hornoch K., Votruba V., 2014, A&A, 563, L9

Darnley M. J. et al., 2016, ApJ, 833, 149

Dobrzycka D., Kenyon S. J., 1994, AJ, 108, 2259

Drake J. J. et al., 2009, ApJ, 691, 418

Drake J. J. et al., 2021, ApJ, 922, L42

Enoto T. et al., 2021a, Astron. Telegram, 14850

Enoto T. et al., 2021b, Astron. Telegram, 14864

Evans P. A. et al., 2007, A&A, 469, 379

Evans P. A. et al., 2009, MNRAS, 397, 1177

Fajrin M., Imaduddin I., Malasan H. L., Arai A., Shinnaka Y., Kawakita H., 2021, Astron. Telegram, 14909

Ferrigno C. et al., 2021, Astron. Telegram, 14855

Gehrels N. et al., 2004, ApJ, 611, 1005

Hachisu I., Kato M., Luna G. J. M., 2007, ApJ, 659, L163

Henze M. et al., 2018, ApJ, 857, 68

H. E. S. S. Collaboration et al., 2022, Science, 376, 77

Hirosawa K., 2006, IAU Circ., 8671, 1

Hjellming R. M., van Gorkom J. H., Seaquist E. R., Taylor A. R., Padin S., Davis R. J., Bode M. F., 1986, ApJ, 305, L71

Kahabka P., van den Heuvel E. P. J., 1997, ARA&A, 35, 69

King A. R., Pringle J. E., 2009, MNRAS, 397, L51

King A. R., Osborne J. P., Schenker K., 2002, MNRAS, 329, L43

Krautter J., 2008, in Bode M. F., Evans A., eds, Classical Novae, 2nd edn. Cambridge Univ. Press, Cambridge, p. 232

Krautter J., Williams R. E., 1989, ApJ, 341, 968

Krautter J., Oegelman H., Starrfield S., Wichmann R., Pfeffermann E., 1996, ApJ, 456, 788

Krimm H. A. et al., 2013, ApJS, 209, 14

Kuin N. P. M. et al., 2020, MNRAS, 491, 655

Leahy D. A., Darbro W., Elsner R. F., Weisskopf M. C., Sutherland P. G., Kahn S., Grindlay J. E., 1983, ApJ, 266, 160

Luna G. J. M. et al., 2021, Astron. Telegram, 14873

Macdonald J., Fujimoto M. Y., Truran J. W., 1985, ApJ, 294, 263

Mason K. O., Córdova F. A., Bode M. F., Barr P., 1987, in Bode M. F., ed., RS Ophiuchi (1985) and the Recurrent Nova Phenomenon. VNU Science Press, Utrecht, p. 167

Mason E., Shore S. N., Drake J., Howell S. B., Kuin P., Magaudda E., 2021, A&A, 649, A28

Mikołajewska J., Shara M. M., 2017, ApJ, 847, 99

Mikolajewska J., Aydi E., Buckley D., Galan C., Orio M., 2021, Astron. Telegram, 14852

Montez R., Luna G. J. M., Mukai K., Sokoloski J., Kastner J. H., 2022, ApJ, 926, 100

Mukai K., 2008, in Evans A., Bode M. F., O'Brien T. J., Darnley M. J., eds, ASP Conf. Ser. Vol. 401, RS Ophiuchi (2006) and the Recurrent Nova Phenomenon. Astron. Soc. Pac., San Francisco, p. 84

Munari U., Valisa P., 2021a, Astron. Telegram, 14840

Munari U., Valisa P., 2021b, Astron. Telegram, 14860

Munari U., Valisa P., 2021c, preprint (arXiv:2109.01101)

Munari U., Valisa P., 2022, preprint (arXiv:2203.01378)

Munari U. et al., 2007, Balt. Astron., 16, 46

Munari U., Valisa P., Ochner P., 2021, Astron. Telegram, 14895

Nelson T., Mukai K., Orio M., Luna G. J. M., Sokoloski J. L., 2011, ApJ, 737, 7

Ness J.-U., 2020, Adv. Space Res., 66, 1202

Ness J.-U. et al., 2007a, ApJ, 665, 1334

Ness J.-U., Starrfield S., Page K. L., Osborne J. P., Beardmore A. P., Drake J. J., 2007b, Progress Theor. Phys. Suppl., 169, 187

Ness J.-U. et al., 2009, AJ, 137, 3414

Ness J.-U. et al., 2015, A&A, 578, A39

Nikolov Y., Luna G. J. M., 2021, Astron. Telegram, 14863

O'Brien T. J., Bode M. F., Kahn F. D., 1992, MNRAS, 255, 683

O'Brien T. J. et al., 2006, Nature, 442, 279

Odendaal A., Meintjes P. J., Charles P. A., Rajoelimanana A. F., 2014, MNRAS, 437, 2948

Orio M., 1993, A&A, 274, L41

Orio M., Behar E., Drake J., Mikolajewska J., Ness J.-U., Osprina N., 2021a, Astron. Telegram, 14906

Orio M. et al., 2021b, Astron. Telegram, 14926

Orio M. et al., 2021c, Astron. Telegram, 14954

Orlando S., Drake J. J., Laming J. M., 2009, A&A, 493, 1049

Osborne J. P., 2015, J. High Energy Astrophys., 7, 117

Osborne J. P. et al., 2011, ApJ, 727, 124

Page K. L., 2021a, Astron. Telegram, 14885

Page K. L., 2021b, Astron. Telegram, 14894

Page K. L., Beardmore A. P., Osborne J. P., 2015, Astron. Telegram, 8133

Page K. L., Beardmore A. P., Osborne J. P., 2020, Adv. Space Res., 66, 1169

Page K. L., Osborne J. P., Aydi E., 2021, Astron. Telegram, 14848

Patterson J., 2011, MNRAS, 411, 2695

Peters W. M., Clarke T. E., Giacintucci S., Kassim N. E., Polisensky E., 2021, Astron. Telegram, 14908

Pizzuto A., Vandenbroucke J., Santander M., 2021, Astron. Telegram, 14851

Prialnik D., Livio M., Shaviv G., Kovetz A., 1982, ApJ, 257, 312

Puckering E. C., 1905, ApJ, 22, 90

Rauch T., 2003, A&A, 403, 709

Ribeiro V. A. R. M., 2012, Mem. Soc. Astron. Ital., 83, 762

Ricra J., Vannini J., Baella N., 2021, Astron. Telegram, 14972

Roming P. W. A. et al., 2005, Space Sci. Rev., 120, 95

Rout S. K., Srivastava M. K., Banerjee D. P. K., Vadawale S., Joshi V., Kumar V., 2021, Astron. Telegram, 14882

Schaefer B. E., 2010, ApJS, 187, 275

Schaefer B. E., 2018, MNRAS, 481, 3033

Schwarz G. J. et al., 2011, ApJS, 197, 31

Schwarz G. J., Page K. L., Kuin P. M., Darnley M. J., 2020, Res. Notes AAS, 4, 142

Shara M. M., 1982, ApJ, 261, 649

Shidatsu M. et al., 2021, Astron. Telegram, 14846

Shore S. N., 2012, Bull. Astron. Soc. India, 40, 185

Shore S. N., Aufdenberg J. P., 1993, ApJ, 416, 355

Shore S. N., Kenyon S. J., Starrfield S., Sonneborn G., 1996a, ApJ, 456, 717

Shore S. N., Starrfield S., Sonneborn G., 1996b, ApJ, 463, L21

Shore S. N. et al., 2021a, Astron. Telegram, 14868

Shore S. N., Teyssier F., Thizy O., 2021b, Astron. Telegram, 14881

Shore S. N., Teyssier F., Guarro J., Allen H., Lecocq V., Shank K., Velez P., 2021c, Astron. Telegram, 14883

Sokoloski J. L. et al., 2006, ApJ, 636, 1002

Sokoloski J. L., Rupen M. P., Mioduszewski A. J., 2008, ApJ, 685, L137

Sokolovsky K. et al., 2021, Astron. Telegram, 14886

Somero A., Hakala P., Wynn G. A., 2017, MNRAS, 464, 2784

Stockman H. S., Schmidt G. D., Lamb D. Q., 1988, ApJ, 332, 282

Taguchi K., Ueta T., Isogai K., 2021a, Astron. Telegram, 14838

Taguchi K., Maehara H., Isogai K., Tampo Y., Ho J., 2021b, Astron. Telegram, 14858

Truran J., Livio M., 1986, ApJ, 308, 721

van den Heuvel E. P. J., Bhattacharya D., Nomoto K., Rappaport S. A., 1992, A&A, 262, 97

van der Klis M., 1988, in Ogelman H., van den Heuvel E. P. J., eds, NATO ASI Series C Vol. 262, Timing Neutron Stars. Kluwer, Dordrecht, p. 27

Vaughan S., Edelson R., Warwick R. S., Uttley P., 2003, MNRAS, 345, 1271

Vaytet N. M. H., O'Brien T. J., Bode M. F., 2007, ApJ, 665, 654

Vaytet N. M. H., O'Brien T. J., Page K. L., Bode M. F., Lloyd M., Beardmore A. P., 2011, ApJ, 740, 5

Verner D. A., Ferland G. J., Korista K. T., Yakovlev D. G., 1996, ApJ, 465, 487

Wagner S. J., 2021a, Astron. Telegram, 14844

Wagner S. J., 2021b, Astron. Telegram, 14857

Walder R., Follini D., Shore S. N., 2008, A&A, 484, L9

Warner B., Woudt P. A., 2002, MNRAS, 335, 84

Williams D., O'Brien T., Woudt P., Nyamai M., Green D., Titterington D., Fender R., Sivakoff G., 2021, Astron. Telegram, 14849

Wilms J., Allen A., McCray R., 2000, ApJ, 542, 914

Wolf W. M., Townsend R. H. D., Bildsten L., 2018, ApJ, 855, 127

Woodward C. E., Evans A., Banerjee D. P. K., Starrfield S., Wagner R. M., Gehrz R. D., 2021a, Astron. Telegram, 14866

Woodward C. E., Banerjee D. P. K., Evans A., Starrfield S., Wagner R. M., Gehrz R. D., 2021b, Astron. Telegram, 14910

Worters H. L., Eyres S. P. S., Bromage G. E., Osborne J. P., 2007, MNRAS, 379, 1557

Woudt P. A., Ribeiro V. A. R. M., eds, 2014, ASP Conf. Ser. Vol. 490, Stella Novae: Past and Future Decades. Astron. Soc. Pac., San Francisco

Wynn G., 2008, in Evans A., Bode M. F., O'Brien T. J., Darnley M. J., eds, ASP Conf. Ser. Vol. 401, RS Ophiuchi (2006) and the Recurrent Nova Phenomenon. Astron. Soc. Pac., San Francisco, p. 73

Yaron O., Prialnik D., Shara M. M., Kovetz A., 2005, ApJ, 623, 398

Zamanov R., Panov K., Boer M., Le Coroller H., 2006, Astron. Telegram, 832

Zamanov R., Stoyanov K., Kostov A., Boeva S., Moyseev M., Marti J., Luque-Escamilla P. L., 2021, Astron. Telegram, 14974

SUPPORTING INFORMATION

Supplementary data are available at *MNRAS* online.

Table 1. Fits to the XRT spectra before (model consisting of two absorbed APEC components) and during (including an additional BB) the SSS phases in 2006 and 2021.

Please note: Oxford University Press is not responsible for the content or functionality of any supporting materials supplied by the authors. Any queries (other than missing material) should be directed to the corresponding author for the article.

This paper has been typeset from a TEX/LATEX file prepared by the author.